BỘ GIÁO DỤC VÀ ĐÀO TẠO

TRƯỜNG ĐẠI HỌC SƯ PHẠM KỸ THUẬT

THÀNH PHỐ HỒ CHÍ MINH

NGUYỄN HUỲNH THI

DANH MỤC CÁC BÀI BÁO ĐÃ CÔNG BỐ

1. Ho Van Phuc, **Nguyen Huynh Thi**, Huynh Thanh Cong, Nguyen Van Trang, "A Cfd Simulation On Effects Of Methane/Biogas Ratio On 2-Stroke Free-Piston Linear Engine's Scavenging", *Journal of Technical Education Science No.59 (08/2020) Ho Chi Minh City University of Technology and Education, pp.130-139, 2020.*
2. **Nguyen Huynh Thi**; Nguyen Van Trang; Huynh Thanh Cong; Huynh Van Loc; Dao Huu Huy; Ngo Duc Huy. "A Preliminary Study of a Two Stroke Free-Piston Engine for Electricity Generation". *5th International Conference on Green Technology and Sustainable Development (GTSD)*,2020. *(IEEE)*
3. **Nguyen Huynh Thi**; Nguyen Van Trang; Huynh Thanh Cong; Huynh Van Loc; Dao Huu Huy; Truong Hoa Hiep; Vo Bao Toan. "An Investigation on Power Generation Characteristics of Linear Generator Driven by a Free-piston Engine". *2021 International Conference on System Science and Engineering (ICSSE)*, 2021. *(IEEE)*
4. **Nguyen Huynh Thi**; Nguyen Van Trang; Huynh Thanh Cong; Huynh Van Loc; Dao Huu Huy; Ngo Duc Huy; Truong Hoa Hiep; Vo Bao Toan. "A Study of the Scavenging Process in a Two-stroke Free Piston Linear Engine at Low Velocity Using CFD and DPM". *6th International Conference on Green Technology and Sustainable Development (GTSD)*, 2022. *(IEEE)*
5. **Nguyen Huynh Thi**; Nguyen Van Trang; Huynh Thanh Cong; Dao Huu Huy. "A Preliminary Study of Spark-Ignition System for Free-Piston Linear Engine". *Journal Of Technical Education Science (JTE)*, 2023.
6. **Nguyen Huynh Thi**; Nguyen Van Trang; Huynh Thanh Cong; Dao Huu Huy . "Preliminary Design of a Single-Phase Linear Generator for Free-Piston Engine Application". *From Smart City to Smart Factory for Sustainable Future: conceptual framework, scenarios, and multidiscipline perspectives SCFF24*, 2024. (Scopus)

A CFD SIMULATION ON EFFECTS OF METHANE/BIOGAS RATIO ON 2-STROKE FREE-PISTON LINEAR ENGINE'S SCAVENGING

Ho Van Phuc[1], Nguyen Huynh Thi[2], Huynh Thanh Cong[1], Nguyen Van Trang[2]
[1]*University of Technology, Vietnam National University-Ho Chi Minh City, Vietnam*
[2]*Ho Chi Minh City University of Technology and Education, Vietnam*

Received 28/7/2020, Peer reviewed 3/8/2020, Accepted for publication 4/8/2020.

ABSTRACT

On the work of investigating the effect of methane percentage in biogas on the two-stroke free-piston linear engine (FPLE) power output, a scavenging simulation implementation is required. Although the computational fluid dynamics (CFD) method was recognized as an effective solution, the result may, however, be not precise if the boundary conditions and the gas properties are determined inaccurately. This paper represents a CFD scavenging simulation, in which, a zero-dimensional model for the unsteady flow into the bounce-chamber based on Reynolds transport theorem was built to observe the scavenging's boundary conditions. Simultaneously, the mixture characteristics following methane percentage and temperature are also estimated, in which, 5 circumstances of biogas component: $40\%\ CH_4$, $50\%\ CH_4$, $60\%\ CH_4$, $70\%\ CH_4$, *and* $100\%\ CH_4$ *that will be inputted in CFD modeling afterward. The result shows that although delivered gas mass is enhanced when using low* $\%CH_4$ *biogas, the volumetric efficiency is decreased, particularly from 0.679 to 0.612 when* $\%CH_4$ *vary from 100% to 40% at engine frequency* $f = 50Hz$.

Keywords: *free-piston linear engine; biogas; computational fluid dynamics; scavenging; simulation.*

Abbreviation:

FPLE	free-piston linear engine	CFD	computational fluid dynamics
LMS	least mean squares	BDC	bottom dead center
HCCI	homogeneous charge compression ignition	UDF	user-define function

1. INTRODUCTION

Within the most potential selection for the conventional engine replacement in terms of hybrid vehicles, FPLE attracts a great number of researchers [1-9]. To study whether the FPLE, which is already known for its high efficiency even reaching 50% indicated efficiency under HCCI operation [5], will be compatible with clean fuels namely biogas or not, it is important to consider the effect of biogas on the engine's performance characteristics itself. When the gas properties vary according to the proportion of biogas components and it directly influence the gas exchange process, which is the key process to improving the engine performance, thus, a scavenging examination is a must to be carried out. CFD is one efficient method to execute the work since it solves the Navier-Stokes equation numerically. Since the cylinder structure uses ports to deliver fresh gas, the scavenging process depends on the fresh gas feeding into the bounce-chamber, hence, the scavenging model and the bounce-chamber gas feeding model should be combined. However, the CFD model is extremely complicated if we include the bounce-chamber geometry. Therefore, simplifying the simulation domain that only maintains the cylinder geometry and calculating the bounce-chamber flow characteristics to define boundary conditions is among the most widely-chosen solutions

(***Figure 1***). There have been an increasing number of reports concerning scavenging simulation using CFD [6-9]. The geometry simulation domains of these studies are only the volume of the cylinder which focus on exchanging fresh gas processes. Nonetheless, boundary conditions computation are ambiguous when it comes to not estimated quantity of fresh gas trapped in the bounce-chamber. In this study, a simple zero-dimensional mathematical model based on the Reynolds transport theorem was built to observe the trapped gas in the bounce-chamber before CFD simulation is implemented. Because the bounce-chamber volume is inconstant as a result of the piston motion, the momentum conservation equation for a deforming control volume is applied.

CFD is a branch of fluid mechanics that uses numerical Navier-Stokes equations to handle the streamline of fluid flow as well as the interaction between it and boundary surfaces. This paper uses the finite volume method, which has advantages in memory usage and calculation speed, especially for solving turbulent flows with high Reynolds number. The $k-\varepsilon$ turbulent model is also applied since the main aim of this work is to measure the trapped fresh gas's mass for thermodynamic simulation in further work, which does not need good predictions in the region near boundaries. Besides, a dynamics mesh is also used in which the piston motion is coded based on the UDF library and compiled by a C++ compiler.

Biogas, which is derived from anaerobic digestion of organic materials primarily contains methane (50-75%), carbon dioxide (25-50%), and may exist insignificant amounts of hydrogen sulfide (0.1-0.5%), moisture and siloxanes. When assuming that biogas has only methane and carbon dioxide, the properties of the fluid which is used in CFD simulation must be in corresponding with the variation of methane percentage. Gas properties that directly affect the CFD simulation are density, viscosity. By applying the least mean squares (LMS) technique, these properties are approximated to multivariable functions from discrete data of every individual mixture's elements. These data were collected from [10]. All of these boundary conditions and gas properties will become an input of CFD modeling afterward.

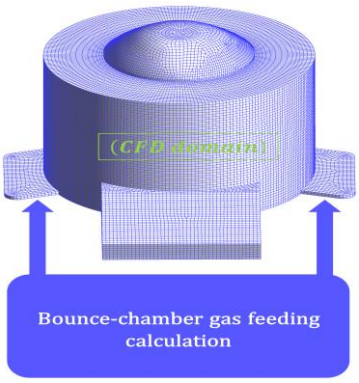

Figure 1. *Simplify the simulation domain.*

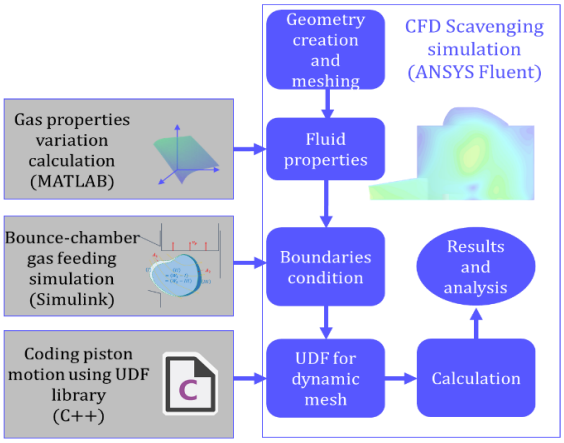

Figure 2. *Illustration of workflow.*

2. MATHEMATICAL MODELLING

2.1 Mixture properties estimate

Density, kinematic viscosity, dynamic viscosity of methane, carbon dioxide, and atmosphere (are collectively referred to as parameter B) are approximated to second-order polynomials with temperature. With the data is discrete $B = \{(T_1, B_1), (T_2, B_2), \dots (T_n, B_n)\}$ fitted to $f(T) = B(T) = \alpha T^2 + \beta T + \gamma$, where T denotes the gas temperature. When the biogas is supposed a mixture of CH_4 and CO_2, the parameter B of biogas is evaluated by:

$$B_{biogas}(T) = \Omega B_{CH_4}(T) + \Psi B_{CO_2}(T) \quad (1)$$

where Ω, Ψ denotes the volumetric percentage of CH_4 and CO_2 component

respectively. The ideal chemical reaction of biogas combustion can be written as:

$$\Omega CH_4 + \Psi CO_2 + 2\Omega\left(O_2 + \frac{79}{21}N_2\right) \xrightarrow{t^0} (\Omega + \Psi)CO_2 + 2\Omega H_2O + \frac{158}{21}\Omega N_2 + Q_{out}$$

According to that, the parameter *B* of the mixture can be determined when the engine is operating at the air-fuel equivalence ratio λ:

$$B_{mix}(T) = \frac{1}{1 + 2\lambda\Omega}\left[B_{biogas}(T) + 2\lambda\Omega B_{atmosphere}(T)\right] \quad (2)$$

2.2 The bounce-chamber gas flow model

The fresh gas must be provided into the bounce-chamber before being pushed by the piston's motion to the combustion chamber via transfer ports. Consequently, the parameters at the end of the bounce-chamber gas feeding process are the boundary conditions for the gas exchange process. The parameter X has the x, which is the amount of *X* per unit mass:

$$X = \iiint x\rho dW \quad (3)$$

where ρ is the gas density, W is the control volume. The time rate of change of X is described below:

$$\frac{DX}{Dt} = \left(\frac{\partial X}{\partial t}\right)_W + \oiint x\rho(\vec{u}\cdot\vec{n})dA \quad (4)$$

where $\vec{n}$ is the unit normal vector, $\left(\frac{\partial X}{\partial t}\right)_W$ is the partial derivative to time of X in the system W while $\oiint x\rho(\vec{u}\cdot\vec{n})dA$ is the net flux of *X* through the control surface A.

With $X = m\vec{u}$ is the flow's linear momentum ($x = \vec{u}$):

$$\frac{D(m\vec{u})}{Dt} = \sum \overrightarrow{F_{external}} = \frac{\partial}{\partial t}\iiint \rho\vec{u}dW + \oiint \rho\vec{u}(\vec{u}\cdot\vec{n})dA \quad (5)$$

Usually, the flow velocity when the engine operating at lower than $5000\ rpm$ is not greater than $100m/s$, which means the Mach number is smaller than 0.3 and, thus, the gas flow is incompressible. Besides, to reduce the complication of the model, the flow streamline is assumed perpendicular to sections $1-1, 2-2$. Since the piston moves at velocity v_p, the control volume is deformed at v_p at the piston bottom surface, hence, relative velocities are used instead. The multiply $(\vec{u}\cdot\vec{n})$ will be equal to $|\vec{u}||\vec{n}|cos\left(\frac{\pi}{2}\right)$ or $|\vec{u}||\vec{n}|cos\left(-\frac{\pi}{2}\right)$ when the flow's streamline is perpendicular to sections and accordingly, it equals either u or $(-u)$ if the gas flow direction is outward or inward the control volume. On the other hand, the velocity profile is nonuniform, the average velocity can be used instead, with the momentum-flux correction factor Γ:

$$\int \rho\vec{u}(\vec{u}\cdot\vec{n})dA = \rho\Gamma\int \bar{u}^2 dA \quad (6)$$

Since the flow is turbulent, leading to Γ varying from 1.01 to 1.04 respectively [11]. These are almost unity that we can normally neglect it ($\Gamma = 1$). The external forces when we ignore the friction between the gas and the wall are the forces due to static pressure at sections. When the piston moves upward:

$$\frac{\partial}{\partial t}\left(\rho\iiint \overline{u_1}W\right) - \rho\iint \overline{u_1}^2 dA_1 = p_1A_1 - \frac{\partial}{\partial t}\left(\rho\iiint \overline{v_p}W\right) \quad (7)$$

When the piston moves downward:

$$\frac{\partial}{\partial t}\left(\rho\iiint \overline{u_1}W\right) - \rho\iint \overline{u_1}^2 dA_1 = p_1A_1 + \frac{\partial}{\partial t}\left(\rho\iiint \overline{v_p}W\right) - \rho\iint \overline{u_2}^2 dS \quad (8)$$

where $u_2 = \frac{A_1}{S}u_1 + v_p$ and all pressures used in this paper are gauge pressure.

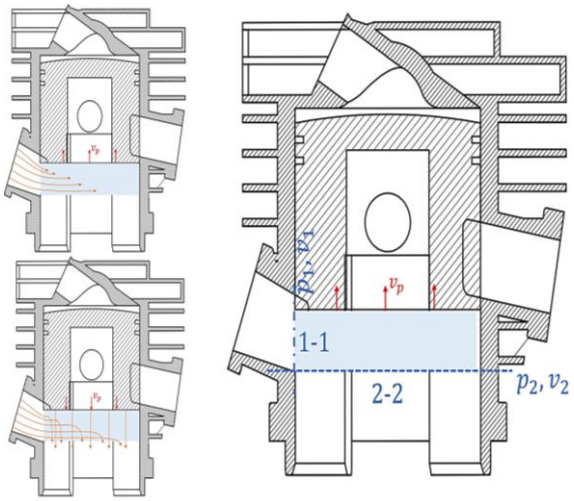

Figure 3. *Cross-section of the cylinder.*

3. SIMULATION

3.1 Boundaries determination

Table 1. *Engine's important parameters.*

Parameters	Unit	Value
Piston diameter	mm	45
Piston displacement	mm	31
Cylinder volume	cm^3	49.3
Piston displacement that intake port is opened	mm	11.7
Piston displacement that transfer ports are opened	mm	6.3
Bounce-chamber volume	cm^3	58.3

The model was built via Simulink, in which the cylinder dimensional parameters are coded in a script file. Important parameters of the modeled engine are listed in the table below. The model calculates separately for piston upward and downward, then the velocity is merged into one signal to integrate with time to obtain the supplied gas quantity. Because the model is segregated, the last value in the piston upward subsystem is driven to initial condition for the piston downward subsystem. The duration of piston downward and upward is controlled by the piston displacement and the sign of the piston velocity. When the piston bottom completely closes the intake port, the simulation is triggered to stop.

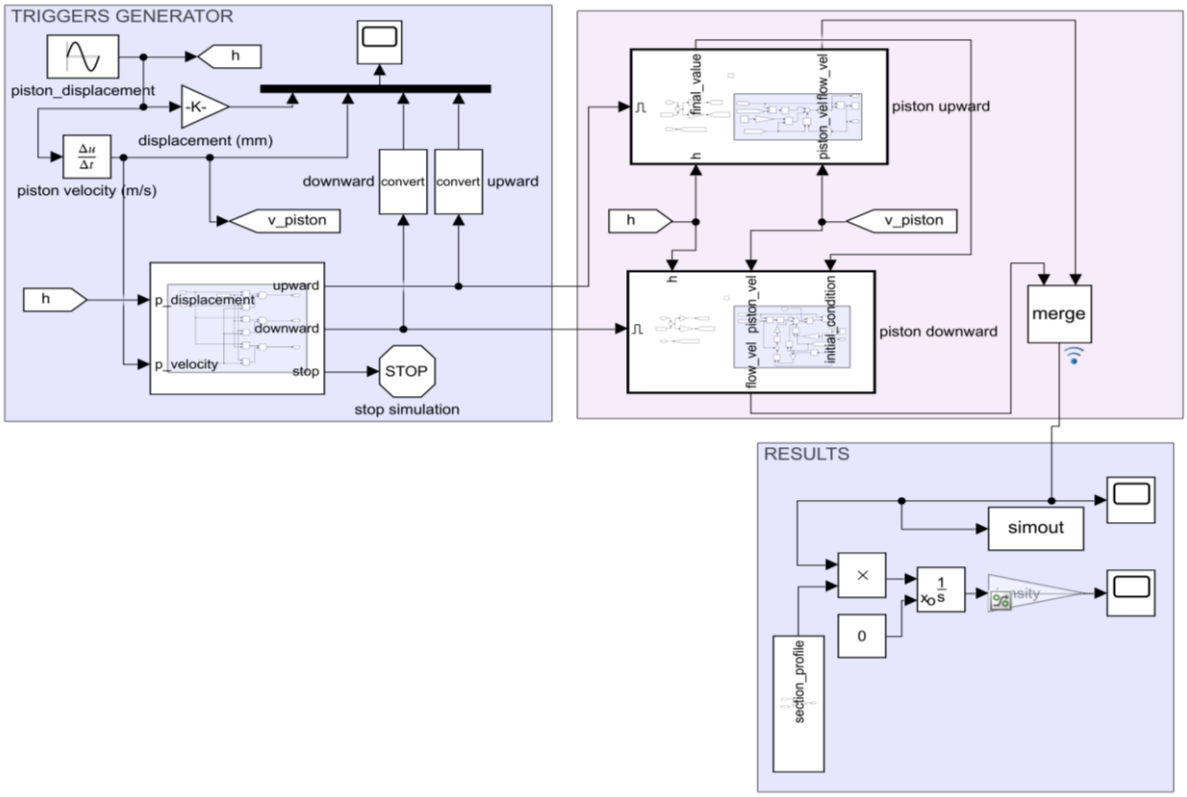

Figure 4. *Modeling for bounce-chamber gas feeding period using Mathworks Simulink.*

3.2 Meshing methodology

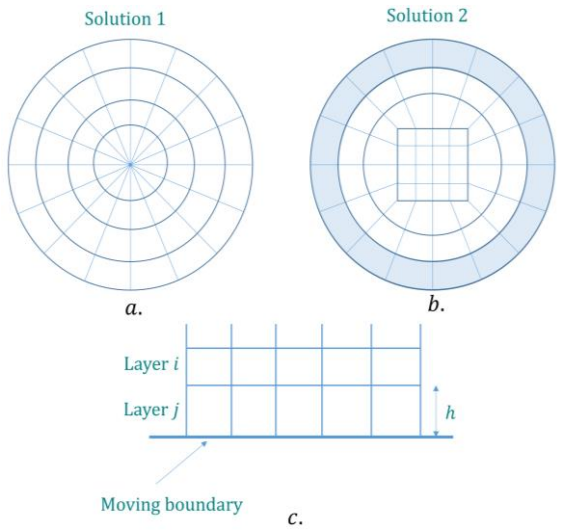

Figure 5. *Solutions for cylinder meshing: a) solution 1. b) solution 2. c) layering method.*

The CFD simulation domain is divided into a large number of cells, which this work is well-known as meshing. With the cylindrical geometry of the combustion chamber, the idea is using hexahedron or prism cells. It arrives at the solution 1 (***Figure 5a***), in which triangular prism cells contact each other at the cylinder's center and are surrounded by tetragonal prism cells. However, the exhaust pipe can not be meshed using prism cells, leading to impossible sharing topology between the cylinder and the exhaust pipe. In solution 2 (***Figure 5b***), a subdomain which contains square prism cells is created, so it allows using both prism cells and hexahedron cells (the blue area) in cylinder geometry. The solution 2 permits connecting the cylinder's mesh and exhaust pipe's mesh since hexahedron cell type is applied in the exhaust pipe.

The piston motion is divided into steps that the mesh updating in every time step is obligated. Since the motion of the piston is perpendicular to the piston top's plane, the layering method is chosen. The layer of cells adjacent to the moving boundary (layer j) is split or merged with the next layer (layer i). If the layer j is expanding, the height of cells in it increases until: $h_{min} > (1 + \alpha_s)h_{ideal}$, where h_{min} is the minimum height of cells in layer j, h_{ideal} is the ideal cell height, and α_s is the split factor. Two new layers are created with their height respectively is h_{ideal} and $(h - h_{ideal})$ or the ratio of their height is equal α_s. On the contrary, if the layer j is being compressed, it can be compressed until: $h_{min} < \alpha_c h_{ideal}$, where α_c is collapse factor. When the condition is met, layer j and i are merged.

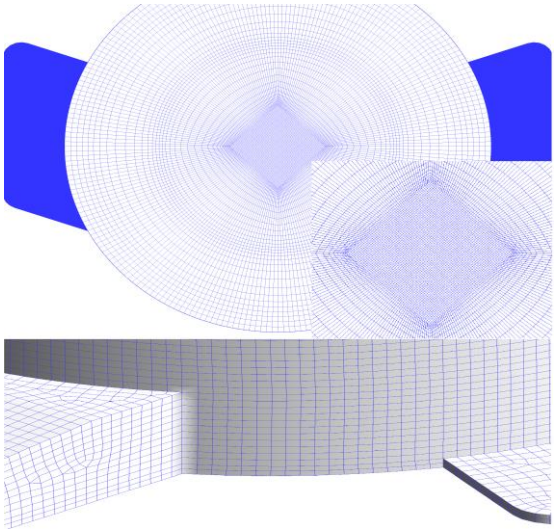

Figure 6. *Applied the solution 2.*

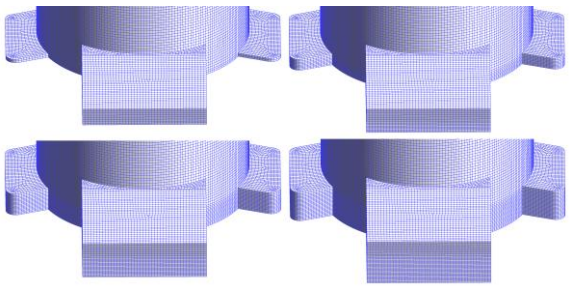

Figure 7. *The mesh updated by using the layering method.*

4. RESULTS AND DISCUSSION

4.1 Gas characteristics

The result in ***Figure 8*** shows that when the $\%CH_4$ increases, although the density of biogas increases, the ideal mixture's density decreases. This is the reason that the more C molecules in biogas, the more oxidative molecules are required. The graph demonstrates the mixture's dynamics viscosity is not affected much by $\%CH_4$ in the region of $20\%CH_4$ to $100\%CH_4$, but by

the temperature. The ideal mixture' characteristics at the atmosphere temperature $30°C$ was collected for 5 circumstances of biogas component: $40\%\ CH_4$, $50\%\ CH_4$, $60\%\ CH_4$, $70\%\ CH_4$, and $100\%\ CH_4$ (***Figure 9***). These values will be saved as the input database for fluid declaration in CFD modeling afterward.

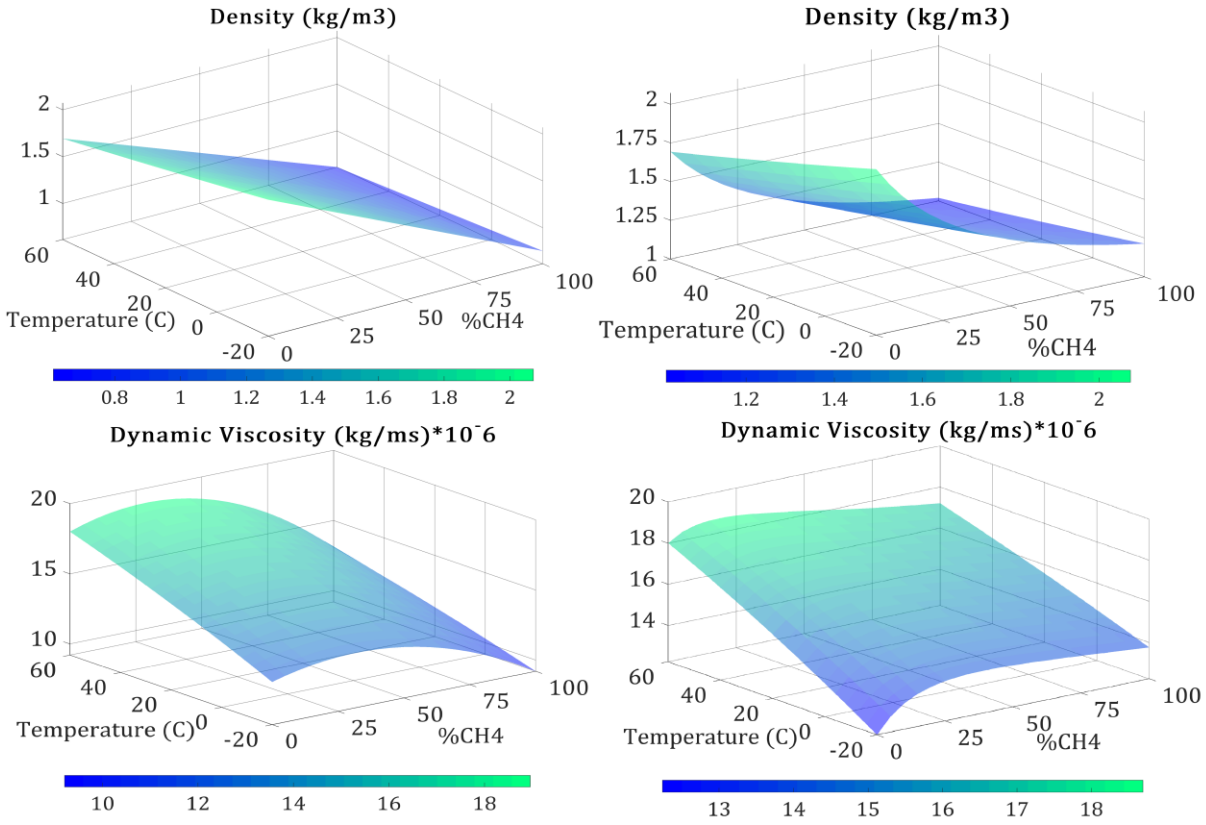

Figure 8. *Density, viscosity (up to down respectively) of biogas (left) and the ideal mixture (right) corresponding to $\%CH_4$ and temperature.*

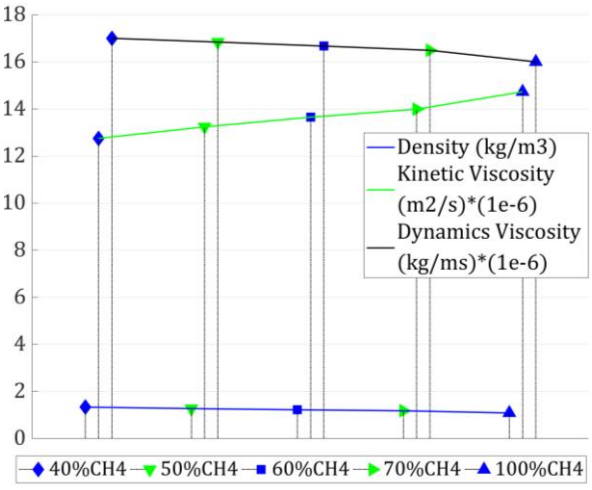

Figure 9. *Density, kinetic viscosity, and dynamic viscosity of ideal mixture variation at $30°C$.*

4.2 Bounce-chamber gas feeding results

The gas flow velocity at the intake port's section is shown in ***Figure 10***, in which the time $0ms$ relates to the piston top at BDC. The velocity shape expresses that the gas was pulled by the piston acceleration during piston moving upward before being pushed by the inertia itself during piston moving downward. The trapped mass of gas in the bounce-chamber is also shown in ***Figure 11***. The result indicates that at the engine's frequency equals $16.67Hz$ (equivalent $1000rpm$ at conventional engine), the delivered gas quantity is exceedingly low (0.0353 gram) bringing the maximum volumetric efficiency can be achieved in

scavenging process at only 0.5395 (when using 40% CH_4 biogas) and therefore, it may be unable to operate the engine. Besides, volumetric efficiency can reach 0.7386 when the engine operates at frequency 83.33Hz (equivalent $5000rpm$).

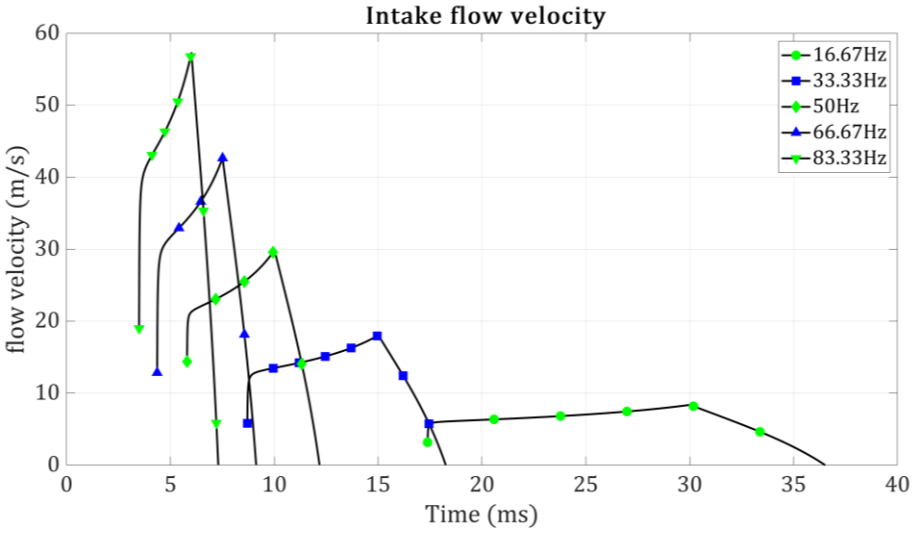

Figure 10. *Flow velocity at the intake port section.*

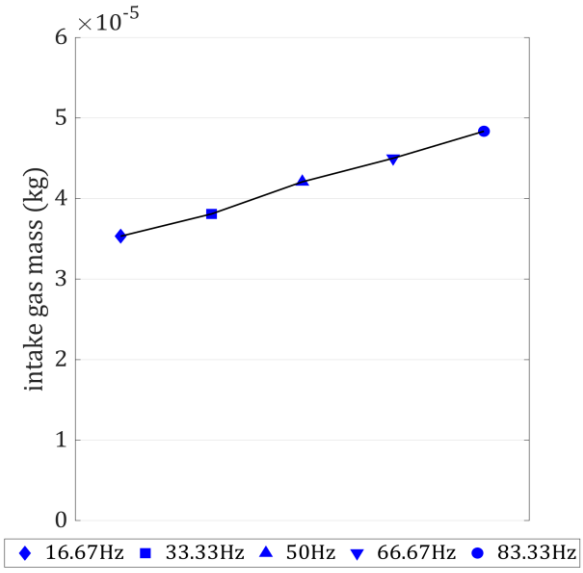

Figure 11. *Quantity of fresh gas into the bounce-chamber.*

4.3 CFD simulation results

The velocity vector field is shown in ***Figure 12***, in which the methane percentage in biogas was set to 40%. A high – speed and great directed tumble comes about in the simulation. The combustion efficiency may be enhanced as a consequence of the tumble closer the TDC during the piston moves upward, which helps the flame propagating speed more rapidly. The turbulent flow, which can be seen in ***Figure 13***, is more strong in higher engine frequency (based on flow's streamlines and flow's velocity). Flow's velocity is highest at the transfer port's cross-section ($\approx 160m/s$ at $f = 16.7Hz$, $\approx 190m/s$ at $f = 33.3Hz$ and $\approx 250m/s$ at $f = 50Hz$) while inside the cylinder, velocity range is significantly lower ($\approx 40 - 90m/s$ at $f = 16.7Hz$, $\approx 60 - 120m/s$ at $f = 33.3Hz$ and $\approx 100 - 190m/s$ at $f = 50Hz$). Besides, the in-cylinder pressure at the end of the intake process, which is a parameter to import to the thermodynamics model in further work, is obtained. Especially, it is more important since FPLE needs to control accurately piston motion to assure stable operation. The higher in-cylinder pressure, the more energy needed for compression. The pressure distribution is shown in ***Figure 14***. When the engine operates at 16.6Hz, the pressure $p_a \approx 1.012\ bar$, and it is higher at engine frequency $f = 33.3Hz$ ($p_a \approx 1.04\ bar$) and engine frequency $f = 50Hz$ ($p_a \approx 1.08\ bar$). The pressure is slightly lower at the center cylinder due to the turbulent phenomenon.

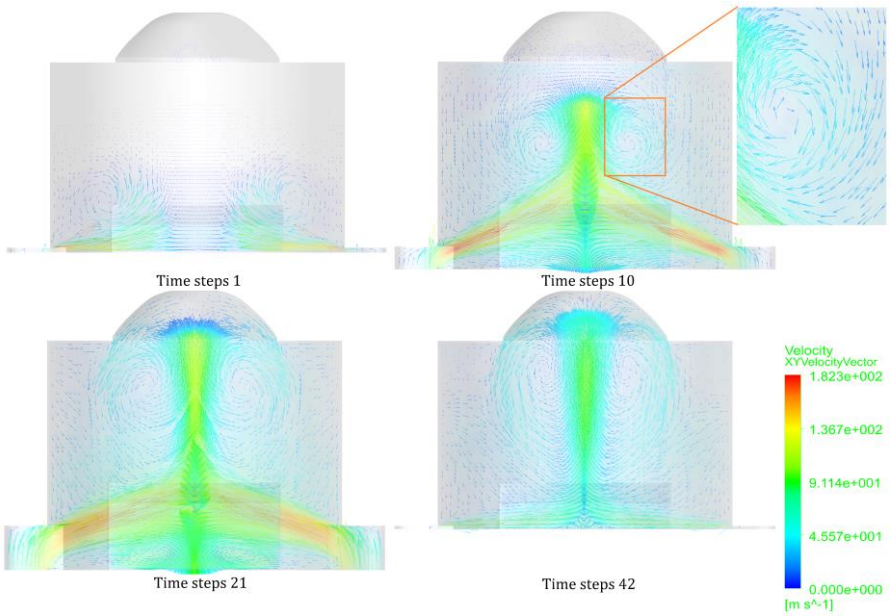

Figure 12. *The velocity vector field at the cylinder cross-section when the engine operates at 16.6Hz fueled with* 40% $CH4$ *biogas.*

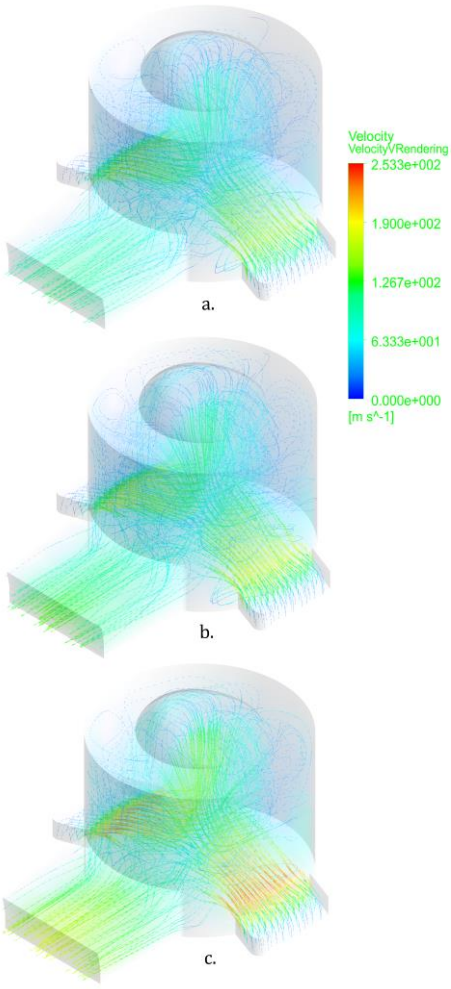

Figure 13. *The velocity streamlines at engine frequency: a. 16.6Hz b. 33.3Hz c. 50Hz.*

Figure 15 shows how the mass flow rate is influenced by time during intake at engine frequency 50Hz. It demonstrates that using biogas which have 40% CH_4 will have the highest mass flow rate. The mass flow rate is rapidly decreasing at the beginning in which the piston top just opens transfer ports, and then grows again. This is due to the open sectional area is still small, and thus, reversed flows can appear as a result of contact between flows and boundaries. ***Figure 16*** shows the delivered gas mass into the cylinder at engine frequency 16.6Hz, 33.3 Hz and 50Hz for 5 circumstances of biogas component proportion 40% CH_4, 50% CH_4, 60% CH_4, 70% CH_4, 100% CH_4. The effect of methane percentage can be easily seen, which the more methane quantity in biogas, the less gas mass delivered into the cylinder. The maximum gas mass is 0.0403 gram when the engine operates at $f = 50Hz$ and fueled with 40% CH_4. However, the intake efficiency is increased following the %CH_4 augmentation (***Figure 17***), particularly from 0.612 to 0.679 when %CH_4 vary from 40% to 100% at engine frequency $f = 50Hz$. This is because of the mixture density decreases when we increase %CH_4.

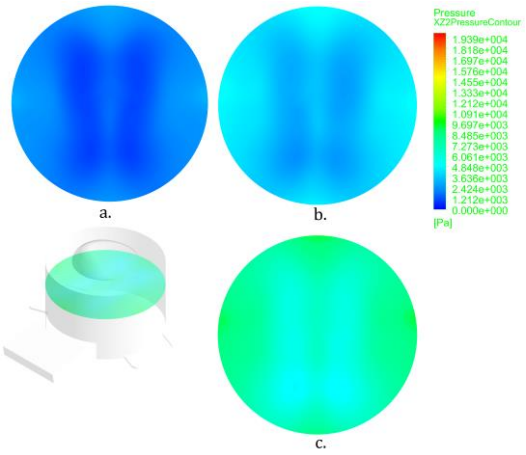

Figure 14. *In-cylinder pressure distribution at the end of scavenging when using 40%CH4 biogas: a. engine operates at 16.6Hz b. engine operates at 33.3Hz c. engine operates at 50Hz.*

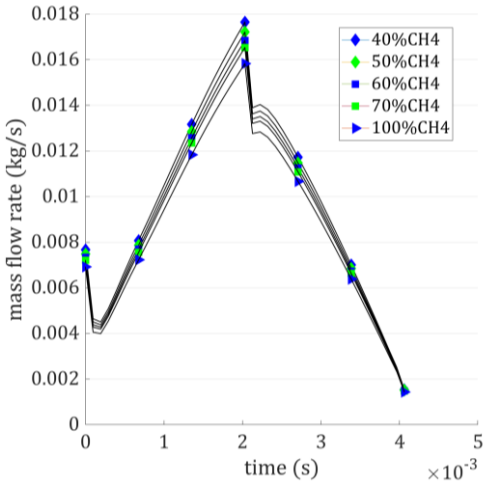

Figure 15. *The mass flow rate at the transfer port's section at engine frequency $f = 50Hz$.*

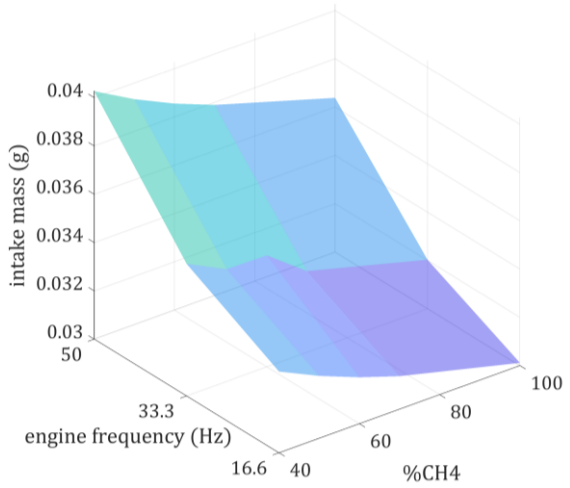

Figure 16. *Delivered gas mass into the cylinder.*

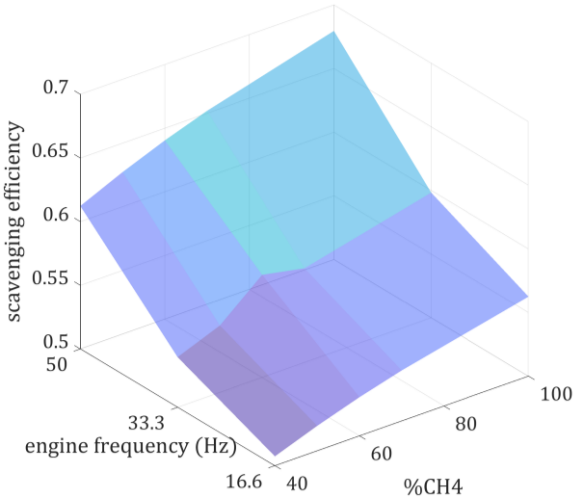

Figure 17. *The map of volumetric efficiency.*

5. CONCLUSION

A CFD scavenging simulation in a two-stroke free-piston linear engine fueled with biogas has been successfully modeled, in which, the boundary conditions are determined based on a zero-dimensional model. Simultaneously, the variation of fresh gas characteristics has been completely observed to be used as the fluid in CFD modeling. The result shows that although delivered gas mass is enhanced when using low $\%CH_4$ biogas, the intake efficiency is decreased, particularly from 0.612 to 0.679 when $\%CH_4$ vary from 40% to 100% at engine frequency $f = 50Hz$.

In the next work, using CFD software to simulate scavenging in FPLE is continued for other lambda circumstances. Then, the thermodynamics model will be built to explore the effect of methane percentage in biogas on the engine power output.

REFERENCES

[1] Boru Jia, Z. Zuo, A. Smallbone, H. Feng, A. P. Roskilly. (2017). A Decouple Design Parameter Analysis for Free Piston Engine Generators. *energies*.

[2] H. Kosaka, T. Akita, K. Moriya, S. Goto, Y. Hotta, T. Umeno, K. Nakakita. (2014). Development of Free Piston Engine Linear Generator System Part 1 - Investigation of Fundamental Characteristics. *SAE Technical Paper*.

[3] H. Kosaka, T. Akita, K. Moriya, S. Goto, Y. Hotta, T. Umeno, K. Nakakita. (2014). Development of Free Piston Engine Generator Part 2 - Investigation of Control System for Generator. *SAE Technical Paper*.

[4] R. Mikalsen, A. P. Roskilly. (2008). The design and simulation of a two-stroke free-piston compression ignition engine for electrical generation. *Applied Thermal Engineering*, 589-600.

[5] P. V. Blarigan, N. Paradiso, S. Goldsborough. (n.d.). Homogeneous Charge Compression Ignition with a Free Piston: A New Approach to Ideal Otto Cycle Performance. *SAE Technical Paper*.

[6] Nguyen Ba Hung, Sung Jaewon, Ocktaeck Lim. (2017). A study of a scavenging process in a two-stroke free piston linear engine using CFD. *9th International Conference on Applied Energy* (pp. 1354-1360). Cardiff, UK: Elsevier Ltd.

[7] S. G. Karunanidhi, Nithin V. S, G. Subba Rao. (2014). CFD studies of two-stroke petrol engine scavenging. *Journal of Engineering Research and Application*, 74-79.

[8] Xuetian Lu, Fujun Zhang, Yuhang Liu, Sufei Wang. (2018). Analysis on Influences of Scavenging Ports Width to Scavenging Process Based on Opposed Piston Two Stroke Diesel Engine. *10th International Conference on Applied Energy* (pp. 5838-5843). Hong Kong: Elsevier Ltd.

[9] Yining Wu, Yang Wang, Xudong Chen, Shuai Guan, Jiancai Wan. (2014). Three dimensional CFD (Computational fluid dynamics) analysis of scavenging process in a two-stroke free-piston engine. *Energy 68*, 168-173.

[10] Retrieved from Engineering Toolbox: www.engineeringtoolbox.com

[11] White, F. M. (2009). Integral Relations for a Control Volume. In *Fluid Mechanics* (p. 165). McGraw-Hill.

Corresponding author:
Ho Van Phuc
University of Technology, Vietnam National University-Ho Chi Minh City
Email: 1870363@hcmut.edu.vn

A Preliminary Study of a Two Stroke Free-Piston Engine for Electricity Generation

Nguyen Huynh Thi
Faculty of Vehicle and Energy Engineering,
Ho Chi Minh City University of Technology and Education
Ho Chi Minh City, Vietnam
nguyenhuynhthi@tgu.edu.vn

Nguyen Van Trang
Faculty of Vehicle and Energy Engineering,
Ho Chi Minh City University of Technology and Education
Ho Chi Minh City, Vietnam
trangnv@hcmute.edu.vn

Huynh Thanh Cong
Vietnam National University-Ho Chi Minh City
Ho Chi Minh City, Vietnam
htcong@hcmut.edu.vn

Huynh Van Loc
Faculty of Industrial Engineering,
Tien Giang University
My Tho City, Vietnam

Dao Huu Huy
Faculty of Vehicle and Energy Engineering,
Ho Chi Minh City University of Technology and Education
Ho Chi Minh City, Vietnam
dhhuy2310@gmail.com

Ngo Duc Huy
Faculty of Vehicle and Energy Engineering,
Ho Chi Minh City University of Technology and Education
Ho Chi Minh City, Vietnam

***Abstract*— Vehicle contributes greatly to the rapid and strong economic development and other aspects of society. Besides, the operation of the transport impact on health and the environment seriously. Therefore, the study of solutions to improve fuel efficiency and environmental protection is one of the most focusing issues. The main objective of this paper is to present the theoretical fundamentals related to the design and development of a two-stroke free-piston engine (FPE) for electrical power generation. In this study, the prototype engine has been conducted with a power of 1.5kW, a bore size of 34mm, and a maximum possible stroke of 28mm using gasoline as fuel. In the future, this engine will be going to take advantage of excess biogas to generate electricity for production activities and daily life. The research has completed the initial intentions such as a theoretical investigation, calculation, determination of the engine model, and starting mechanism. Preliminary results have confirmed the feasibility of proposing the FPE model.**

Keywords*— Free-piston engine, internal combustion engine, linear generator; starting system

I. INTRODUCTION

In recent years, along with the increase in population and the growth of economies, there has been a rapid increase in the number of private vehicles. When working, internal combustion engines emit many components that pollute the environment such as carbon dioxide (CO_2), carbon monoxide (CO), nitric oxides (NO and NO_2), sulfur dioxide (SO_2), hydrocarbons and this substance in high concentrations will directly affect human health, the environment, and the atmosphere. This is one of the great challenges for the fields of internal combustion engines, energy, and the environment. Due to the limitations of fossil fuel and stricter emissions standards, conventional engines tend to replace by more efficient engines. FPE considers the solution with the advantages of reducing NOx emissions [1], multi-fuel [2], and high performance [3]. The absence of crankshaft makes the structure of FPE simple, reducing friction compared to conventional engines [4].

In recent years, many research groups are working on FPE prototypes as an alternative to conventional engines [5-7, 19]. However, most prototypes are often complicated to control. To overcome these problems, a FPE prototype with a dual-piston configuration was proposed, by eliminating the generator, mechanical starting system, fixing top dead center (TDC) make it easy to manage some simple operating conditions.

II. DEVELOPMENT OF ENGINE PROTOTYPE

FPE is the engine that converts from thermal energy to electric energy. FPE has variable compression ratio capability, thus it is suitable for multi-fuel operation [8]. Moreover, its high efficiency and quick transient response make it suitable for hybrid electric vehicle applications [9]. Currently, FPE configurations include single piston, dual piston, and opposed piston. However, the dual-piston configuration is capable of providing high performance despite being a relatively simple device [10]. This paper proposed a simple engine prototype of dual piston configuration in Fig. 1. The structure of the prototype includes two-chamber combustion, mechanical starting system, and driveshaft.

The engine works on the principle of the heat release of the first combustion chamber will create compression pressure in the second combustion chamber, then combustion chamber 2 will release heat by burning fuel with spark and continuous process. The main shaft brings the generator moved freely between two consecutive processes of heat release from two combustion chambers thereby generating electricity. In a dual piston configuration the heat release of the first piston greatly affects the second piston because the FPE is not restricted by the crankshaft connecting device, the piston dead center is not fixed. Therefore, without proper control, it can lead to a collision between the piston and cylinder head, and the unstable compression ratio can lead to deviations [11-12]. Therefore, mechanical mechanisms that

manage the top dead center (TDC) and bottom dead center (BDC) was proposed to prevent the engine from losing control [18]. By eliminating the linear alternator, which will be replaced by a mechanical starting system that is easy to control.

The prototype uses two 2-stroke engines at both ends with a bore size of 34 mm and a piston stroke of 28 mm, the highest compression ratio is 7.5:1. The simple design of the free piston engine and the reduced number of moving parts minimize frictional losses as in Fig. 2. The crank mechanism will be eliminated, and the piston friction is reduced due to the purely linear motion, giving low side forces on the piston.

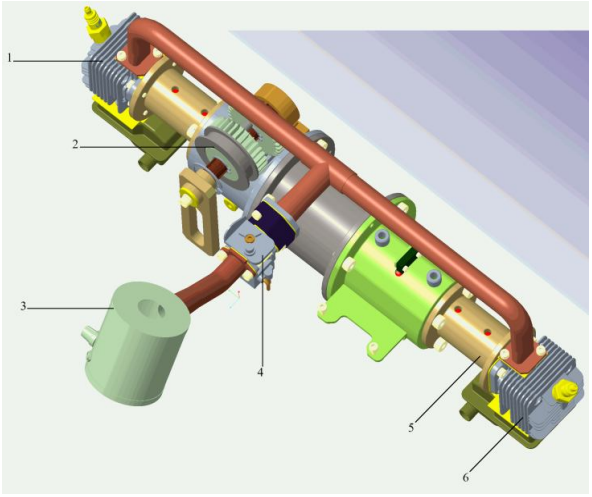

Fig. 1. A prototype of two-stroke free piston engine.

1- Cylinder 1; 2- Activation mechanism; 3- Compressor; 4-Carburetor, 5-Compressed air chamber; 6-Cylinder 2

A compressor is arranged to compress the air and fuel mixture into the compression chamber, the opening and closing of the discharge port and intake port will depend on the piston movement. The working cycle of the engine is composed of compression, combustion, expansion, and scavenging.

III. Conceptual Design of Free-Piston Engine (FPE)

A. *Thermodynamic cycle of FPE*

The two-stroke engines work on the Otto cycle [13] which includes: two isochoric processes and two adiabatic processes. However, the correlation of the timing of every process differs from the four-stroke engine, and it depends on the cylinder's structure, which is the position of the transfer port and the exhaust port that showed in Fig. 2. The diameter of the cylinder is D; the intake port diameter is D_i and the exhaust port diameter is D_e; D_t is the transfer port size; S is the stroke length; S_t is the distance from the top dead center to the point starting open the transfer port; S_e is the distance from the top dead center to the point starting open the exhaust port; *a* is the point which the intake process begins; *r* is the compression process beginning point; *c* is the point which spark-plug ignites; *z* is the point which the cylinder's pressure reaches maximum p_z, and b is the beginning point of an exhausting process.

Assuming that the changing of the cylinder's pressure in the scavenging period is inconsiderable, it means that $p_r \approx p_a$. The thermodynamic calculation starts at the point r with the error of residual gas temperature T_r less than 1%.

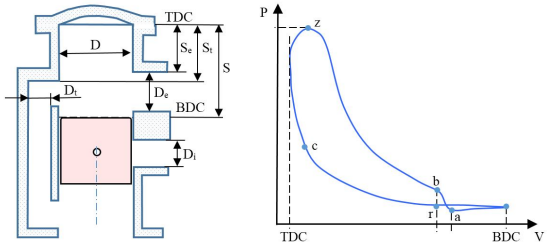

Fig. 2. Engine structure and the theoretical Otto cycle.

TABLE I. Free-Piston Engine Specifications

Number of cylinder	1
Type of engine	2 stroke
Bore	34 mm
Stroke	28 mm
Moving mass	0.58 kg
Nominal compression ratio	7.5:1
Fuel	gasoline

B. *Simulate compressive pressure in the cylinder*

Application in cylinders can be assessed by the derivative form of the first law of thermodynamics. The simulation will be based on Matlab/Simulink program.

$$\frac{dy}{dx} = -\gamma.\frac{p}{V}.\frac{dV}{dt} + (\gamma - 1)\frac{Q_{in}}{V}\frac{dx_b}{dt} \quad (1)$$

P is pressure in cylinder (MPa); γ is the specific heat ratio; V is volume (m^3); Q_{in} is the input heat energy; x_b is mass of burned mixture.

The combustion process, which simulates the mass fraction burned, is performed by the Wiebe function [13-14,18].

$$x_b = 1 - exp\left[-a\,.\,\left(\frac{t-t_s}{c_d}\right)^{b+1}\right] \quad (2)$$

C_d is the combustion duration; t_s is ignition time. The constants of a = 5, and b = 2.

The simulation base on initial pressure taken from experiment 4.5 (kg/cm^2); ignition time at 2 mm before TDC; Stoichiometric air – fuel ratio, $\lambda \approx 1$; engine speed of 10 Hz The results in Fig. 3 shows the relation between velocity and piston position displacement for mentioned compression ratios. The parameters change, but the curves keep the same shape. A larger compression ratio may lead to a bigger velocity and moving frequency.

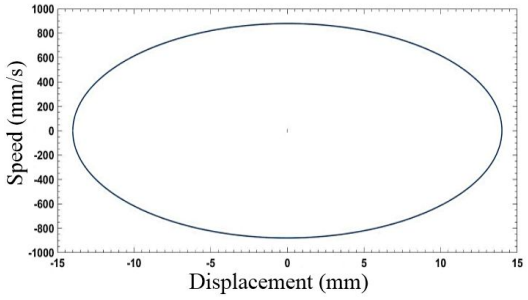

Fig. 3. The displacement corresponds to the velocity of the piston.

Simulation results can achieve pressure greater than 10 kg/cm^2 with the burn time (t-ts) 20 ms that can be shown in

Fig 4. Basing on the maximum pressure value, the ignition timing can be determined.

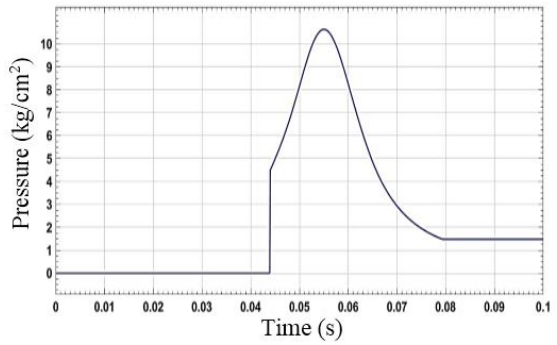

Fig. 4. Graph of peak pressure

IV. Conceptual Design Of The Mechanical Starting System

To startup, the FPE must be set to a certain frequency [15-17] to create pressure in the cylinder. Therefore, a mechanical starting system has been proposed with a simple control instead of a linear motor, to ensure piston displacement illustrated Fig. 5. The rack and pinion gears are used to convert rotational motion into reciprocating linear motion, a DC motor with a power of 500 W drive the driven gear to force the rack connected to the main shaft.

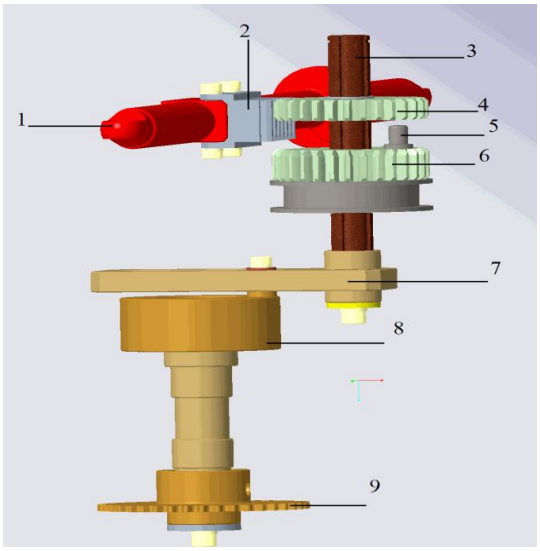

Fig 5. Mechanical starting mechanism.

1 - Main shaft; 2 - Rack; 3 - Shaft of starting mechanism, 4 - Driven gear; 5 - Fasteners; 6 - Drive gear; 7 - Handwheel; 8 - Eccentric wheel; 9 - Driven Gear from Starter Gear of Starter Motor.

The drive gears are linked to the rack and the main shaft when the main shaft moves the drive gear to determine the position of the main shaft. The driven gear is connected to the driven gear from the starter gear of the starter motor. When the driven gear and drive gear are interlocked through the fasteners, the force from the motor through the eccentric gear reaches the starting shaft and drives the main shaft. Moreover, the starting speed can be easily controlled by a motor controller that allows for starting of the engine at each different speed.

The rack pinion mechanism helps to manage TDC and BDC of the piston when starting the engine. The displacement is 26 mm smaller than the maximum stroke of 28 mm, due to the reserve for inertial forces and mechanical errors. From the geometric method, design parameters can be shown in Fig. 6.

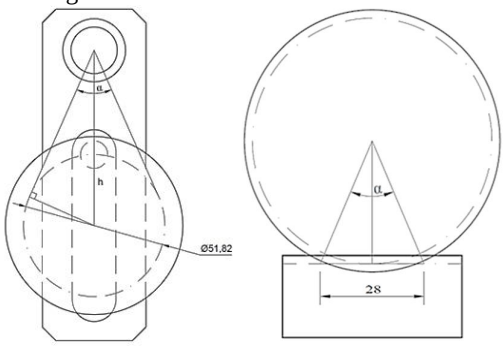

Fig. 6. The rack pinion mechanism of starting system.

V. Results and Disscussion

The start-up process must ensure that sufficiently high pressure is maintained to allow the fuel to ignite. Thus, the engine must reach high speed and large torque to overcome friction, compression pressure at both ends of the cylinder. The experimental model of the mechanical starting system is established in Fig. 7.

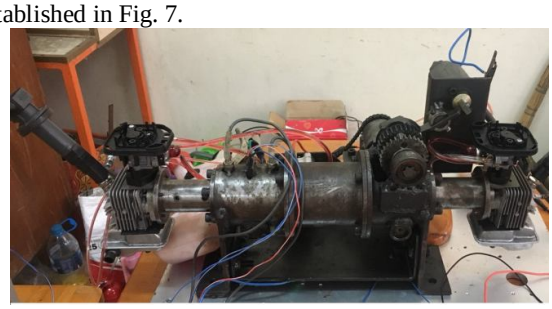

Fig. 7. Experimental model of PFE

Fig. 7 shows the starting system mechanism, the DC motor can achieve a maximum speed of 0.4 m/s with a frequency of about 5 Hz. However, the speed can be changed by changing gear size or gear ratio between the number of teeth on the driven and drive gear.

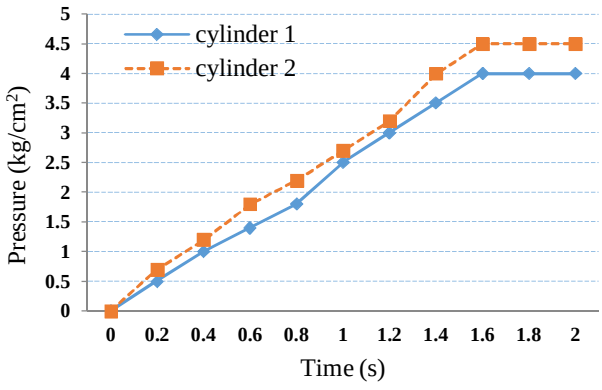

Fig. 8. Compression pressure in the cylinder and starting time

Fig. 9. illustrates the maximum compression pressure in the cylinder reaches 3.5 - 4.5 kg/cm^2 and stable for the rest of

the time, although the engine speed reaches its maximum in about 0.5 seconds, the maximum pressure is reached in about 2 seconds. That shows the maximum compression pressure in a cylinder must have a certain number of oscillations. The maximum pressure between cylinder 1 and cylinder 2 is not equal, which is predictable due to the inertial force in two cylinders which is difficult to control.

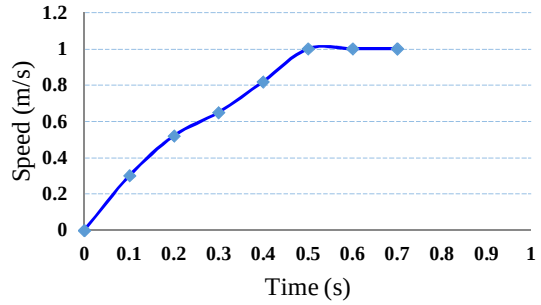

Fig. 9. Piston speed versus starting time

The engine prototype has successfully start up. However, the engine was not working stable, the reason for this is that the probability of misfiring at high engine speed. Misfiring may represent a problem in the free-piston engine since it does not have energy storage capable of driving the engine for several revolutions like the flywheel in a conventional engine [2]. Fig. 10 shows the maximum pressure when successful ignition reaches over 9 (kg/cm^2) when the starting system is still working.

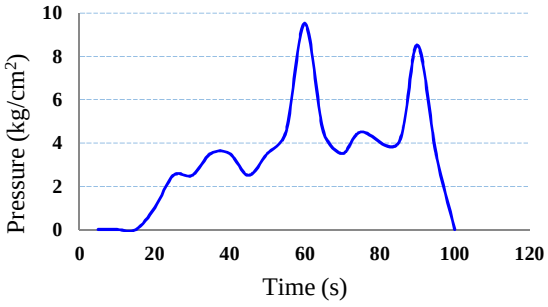

Fig. 10. Peak pressure for successful startup

VI. Conclusions

The paper proposes a simple prototype of FPE with a mechanical starting system. Some preliminary results show that the successful engine startup can be able to obtain at a mean piston speed of 0.4 m/s and a maximum pressure of 4-4.5 (kg/cm^2), the time taken to reach the peak pressure is relatively short in the range of 2 s. The DC motor drive the main shaft of FPE to startup at a stable speed. The pressure at the different cylinder heads is a problem that needs to be solved. The prototype has started a forced ignition test during start-up and has succeeded in a few cycles but requires more optimal research.

A potential challenge with the free-piston design is the engine control strategy. The compression stroke is driven by the power stroke expansion in the opposite cylinder. Variations in the combustion progress in one cylinder will influence the compression and combustion in the other. For the free-piston concept to be feasible, a control system which can secure stable and smooth engine operation must be realized. In the future, lots of additional works must be performed before the FPE prototype comes true.

Acknowledgment

This work belongs to the project grant No: KC-178 funded by Ministry of Education and Training, and hosted by Ho Chi Minh City University of Technology and Education, Vietnam.

References

[1] H. Feng, C. Guo, C. Yuan, Y. Guo, Z. Zuo, A. P. Roskilly, et al., "Research on combustion process of a free piston diesel linear generator," Applied Energy, vol. 161, pp. 395-403, 2016.

[2] R. Mikalsen and A. P. Roskilly, "A review of free-piston engine history and applications," Applied Thermal Engineering, vol. 27, pp. 2339-2352, Oct 2007.

[3] J. Hansson and M. Leksell., "Performance of a Series Hybrid Electric Vehicle with a Free-Piston Energy Converter," IEEE Xplore, 2007.

[4] B. Jia, R. Mikalsen, A. Smallbone, and A. Paul Roskilly, "A study and comparison of frictional losses in free-piston engine and crankshaft engines," Applied Thermal Engineering, 2018.

[5] M. R. Hanipah, R. Mikalsen, and A. P. Roskilly, "Recent commercial free-piston engine developments for automotive applications," Applied Thermal Engineering, vol. 75, pp. 493-503, 2015.

[6] Nguyen Ba Hung, Ock Taeck Lim, "A study of a two-stroke free piston linear engine using numerical analysis," Journal of Mechanical Science and Technology, pp.1545-1557, 2014

[7] Jia B, Tian G, Feng H, Zuo Z, Roskilly AP. "An experimental investigation into the starting process of free-piston engine generator," Apply Energy 2015;157: 798–804.

[8] Q. Li, J. Xiao, and Z. Huang, "Simulation of a two-stroke free-piston engine for electrical power generation," Energy & fuels, vol. 22, pp. 3443-3449, 2008.

[9] R. Mikalsen and A. P. Roskilly, "The control of a free-piston engine generator. Part 1: Fundamental analysis," Applied Energy, pp. 1273-1280, 2010

[10] R. Mikalsen and A. P. Roskilly, "The control of a free-piston engine generator. Part 2: Engine dynamics and piston motion control," Applied Energy, pp. 1281-1287, 2010.

[11] Boru Jia, Zhengxing Zuo, Huihua Feng, Guohong Tian, A. P. Roskilly, "Development approach of a spark-ignited free-piston engine generator,", SAE Technical Paper, No. 2014-01-2894, 2014.

[12] Blair, G. P. Design and Simulation Two-stroke Engine. Society of Automotive Engineers, Inc., 1996.

[13] J. B. Heywood, Internal combustion engine fundamentals, McGraw-Hill Book Company, New York, USA (2018).

[14] Fredriksson J, Bergman M, Golovitchev V, Denbratt I. "Modeling the effect of injection schedule change on free piston engine operation," SAE paper 2006-01- 0449; 2006.

[15] Yitong Jiang a, Daojing Wang, Fushui Liu, Shuwei Zhao, and Qing Yang. "Dynamic Simulation of a Two-Stroke Spark Ignition Free-Piston Engine Generator,". pp 225-230. 2014.

[16] R. Mikalsen, E. Jones, and A. P. Roskilly, "Predictive piston motion control in a free-piston internal combustion engine," Applied Energy, vol. 87, pp. 1722-1728, 2010.

[17] R. Mikalsen, A.P. Roskilly, "The design and simulation of a twostroke free-piston compression ignition engine for electrical power generation," Applied Thermal Engineering (2007).

[18] Jaeheun Kim, Choongsik Bae, Gangchul Kim, "Simulation on the effect of the combustion parameters on the piston dynamics and engine performance using the Wiebe function in a free piston engine," Applied Energy, pp. 446-455, 2014.

[19] Johnson, T., Leick, M., and Moses, R., "Experimental Evaluation of a Prototype Free Piston Engine - Linear Alternator (FPLA) System," SAE Technical Paper 2016-01-0677, 2016.

An Investigation on Power Generation Characteristics of Linear Generator Driven by a Free-piston Engine

Nguyen Huynh Thi
Faculty of Vehicle and Energy Engineering, Ho Chi Minh City University of Technology and Education
Ho Chi Minh City, Vietnam
nguyenhuynhthi@tgu.edu.vn

Nguyen Van Trang
Faculty of Vehicle and Energy Engineering, Ho Chi Minh City University of Technology and Education
Ho Chi Minh City, Vietnam
trangnv@hcmute.edu.vn

Huynh Thanh Cong
Vietnam National University- Ho Chi Minh City
Ho Chi Minh City, Vietnam
htcong@vnuhcm.edu.vn

Dao Huu Huy
Faculty of Vehicle and Energy Engineering, Ho Chi Minh City University of Technology and Education
Ho Chi Minh City, Vietnam
dhhuy2310@gmail.com

Huynh Van Loc
Faculty of Industrial Engineering, Tien Giang University
My Tho City, Vietnam

Truong Hoa Hiep
Faculty of Industrial Engineering, Tien Giang University
My Tho City, Vietnam

Vo Bao Toan
Faculty of Vehicle and Energy Engineering, Ho Chi Minh City University of Technology and Education Ho Chi Minh City, Vietnam

Abstract— **There are many energy sources converted from PMLG (Permanent Magnet Linear Generator- PMLG) linear generator such as wave energy, free-piston engine. This paper proposes the design and study of a single-phase PMLG with a simple structure. Using motion simulators, the objective is to investigate the PMLG's operation at low moving speeds from 0.25 m/s to 0.5 m/s. To determine the electrostatic parameters, a 3-D of linear generator is built-in Ansoft Maxwell V16 software. Using Matlab software, then, these parameters are used to estimate the output basic parameters such as current, voltage, and power that are quantitatively compared with experimental results. The obtained results show that by changing the displacement speed of the linear rod from 0.25 m/s to 0.5 m/s, the voltage and the current increase to double and 10 times, respectively. These results of voltages are also compared with experimental results at speeds of 0.25m/s and 0.5 m/s with and without a load of R_L=3.5Ω. As the displacement speed changes, the voltage increases 2 times (20V to 40V) for the case of without a load and increases about 4 times (4V to 15V) with a load. From this study, the obtained results demonstrate the feasibility of a linear generator driven by a small power free-piston internal combustion engine to generate electricity.**

Keywords— permanent magnet linear generator; Stirling engines, free-piston engine; finite element method – FEM

I. INTRODUCTION

Currently, Permanent Magnet Linear Generators (PMLGs) are consider as potential equipment for practical applications when using variable linear motion instead of the rotary motion as the traditional generator. Since most PMLGs have a simple structure, with little loss in the energy conversion process due to the elimination of redundant transmission devices [1-3]. Nowadays, with the rapid development of high-energy-density magnet materials, PMLG is increasingly being studied for many applications because of their much more efficiency and reliability [4] such as a device converted to electricity with wave energy [5-7], a mechanical energy-to-electrical converter in free piston linear engine (FPLE). Which has the advantages of compactness, high efficiency [8], variable compression ratio should be suitable for many different fuels [9], reducing friction compared to conventional heat engines [10]. Visibly, FPLE is a research trend to improve the performance of hybrid vehicles. Depending on the configuration, frequency, and displacement FPLE has different generating capacities [11-13]. Many studies show that FPLE can be generated electric power at max speed, and achieved in stability operations at low speed using control strategies [14-15]

This paper conducts a design and proposes a single-phase PMLG with a simple structure. Utilizing motion simulators, the objective is to investigate PMLG's operation at low speed from 0.25 m/s to 0.5 m/s – the maximum speed, short displacement of ± 40mm, the output voltage at different speed is a value for data collection and evaluation. The generator is modeled in 3-D by using Ansoft Maxwell V16 (AM-V16) software to obtain the magnetostatic, then simulated by MATLAB software to get output values such as current, voltage, and power to verify with experimental results.

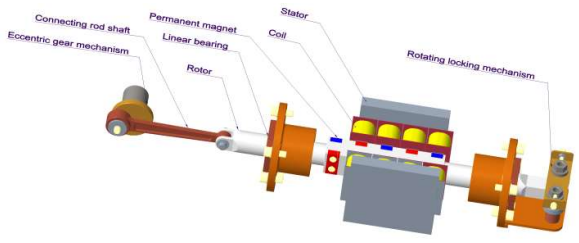

Fig. 1. 3D model structure of a studied generator

The paper presents a flat single phase generator with 2 generating faces, the 3-D structure as shown in Fig. 1, the initial dimensions of the rotor and stator assemblies are shown in Table I and Fig. 2.

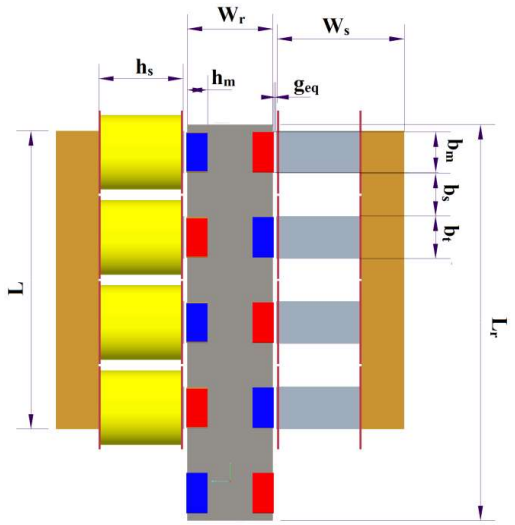

Fig. 2. Cross-section structure of PMLG

TABLE I. GEOMETRIC PARAMETERS OF PMLG

Name	Symbol	Value
- Length of the stator core	L	160 mm
- Stator width	W_s	40 mm
- Slot width	b_s	20 mm
- Tooth width	b_t	20 mm
- Magnets width	b_m	20 mm
- Height of magnets	h_m	10 mm
- Air gap	g_{eq}	1 mm
- Tooth high	h_s	35 mm
- Length of the rotor	L_r	180 mm
- Rotor width	W_r	40 mm
- Number of turns per coil	N	300×8

Similar to a conventional generator PMLG has 2 parts rotor (moving component or mover) and stator. The rotor consists of two sides mounted with polarized permanent magnets, the polarization direction of the permanent magnets is opposite between the two opposite faces and opposite on the same face, to reduce the weight of the rotor so the rotor is made of aluminum. The external stator consists of two multilayer ferrite cores arranged in parallel with two faces mounted with permanent magnets, the clearance between the magnet and the stator is 1mm. Each ferrite core is divided into 4 teeth and the coils are wound around the teeth of the ferrite core. A linear motion is simulated by an eccentric gear mechanism with a displacement of ±40mm. The rotor moves in the horizontal direction by a motor pulling with a capacity of 1.5 HP. The PM part of the motor is made of NdFeB rare earth magnet, the diameter of the copper wire is chosen to be 1.5 mm with 300 turns of wire per tooth.

II. SIMULATION STUDY

A. Theoretical basis

PMLG principle is based on electromagnetic induction and linear motion motor. A magnet mounted on a moving rotor uniformly changes a magnetic field through the coil to generate electromotive force and outputting alternating current. As the winding parameters and core sizes are verified, the electromechanical parameters of the generator play an important role. For this, AM-V16 software is used to solve all the problems of statics. These problems are described by Maxwell's differential equations.

The basic principles of permanent magnet linear generators are related to the magnetic field principle of Maxwell's equations.

According to Ampere's law:

$$\nabla \times H = J \quad (1)$$

where J: current density

H: field intensity

From Gauss law:

$$\nabla \times B = 0 \quad (2)$$

Magnetic flux density B can be related to H as:

$$B = \mu \times H \quad (3)$$

If it is a nonlinear material, the permeability is a function of B:

$$\mu = \frac{B}{H(B)} \quad (4)$$

Flux density B can be expressed in terms of vector potential A as:

$$B = \nabla \times A \quad (5)$$

From equation (4) and (5), yield:

$$\nabla \times \left(\frac{1}{\mu(B)} \times A\right) = 0 \quad (6)$$

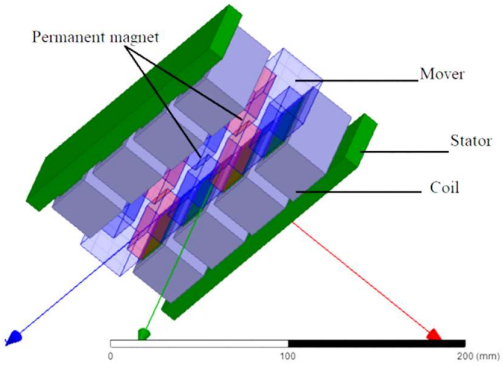

Fig. 3. Studied simulation model using AM-V16

The Finite Element Method (EFM) is a numerical method that allows solving equation (6) used for static problems with nonlinear B-H relationships. Fig. 3 simulated model on Maxwell Ansoft V16, the position of the magnet is placed

parallel to the coil, in this position the magnetic flux through the coil is the largest.

The simulation results in Fig. 4 show that the magnetic flux of the magnet in the actual displacement part is acceptable Br = 1.2 T and Fig. 5, the maximum flux through the coil is 1.3 T and the lines Magnetic force creates a closed circle through the coil, creating an induced electromotive force. Also, the matrix function in AM-V16 is applied for single-phase current to find the synchronous inductance of the coil L_s = 24,404mH.

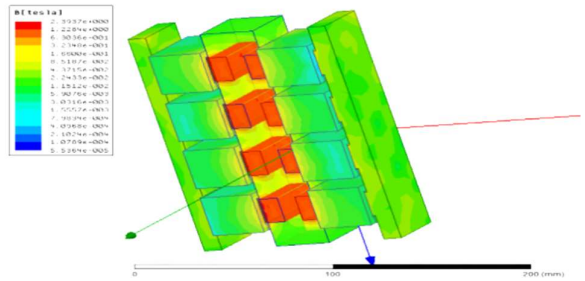

Fig. 4. Surface flux density distribution of PMLG

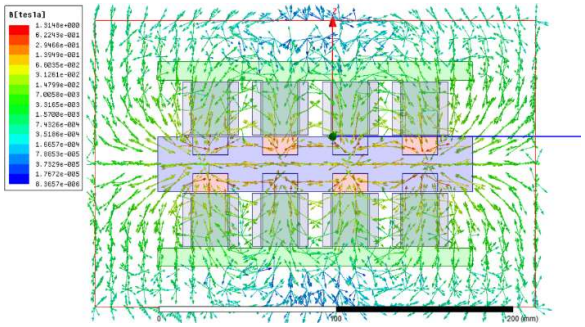

Fig. 5. Direction of vector B

B. Estimation of basic output parameters

The simulation parameters obtained by Finite Elemetn Method (FEM) and the dimension parameters in Table 1 will be entered into Matlab software to simulate the output parameters of the generator. The simulation objective is to find out the speed of generating voltage, the capacity to match the resistive load R_L = 3.5Ω, the armature resistance R_a = 0.25Ω. Thus, analyze the efficiency of a single-phase generator moving at a constant speed using the equivalent circuit of Fig. 6.

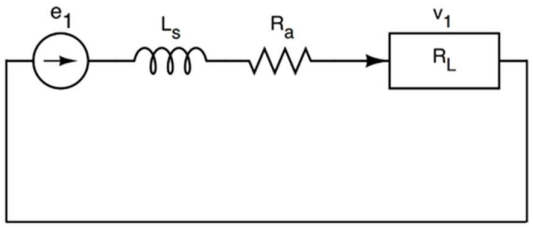

Fig. 6. Equivalent Circuit of single phase Winding of Generator

Carter's coefficient calculates the equivalent clearance [16]:

$$K_c = \frac{\tau_t(5g+b_S)}{\tau_t(5g+b_S)-b_S^2} \quad (7)$$

$$g_{eq} = K_C \cdot ga \quad (8)$$

The air-gap flux density (accounting for increased reluctance) is:

$$Ø = \frac{B_r h_m H_c \mu_0}{h_m H_c \mu_0 - g_{eq} B_r} \quad (9)$$

B_r: Permissible flux density in translator core

H_c =905,000 A/m: Coercive magnetic field intensity

The permeability of free space μ_0 is defined as: $\mu_0 = 4\pi \times 10{-}7$ T.m / A.

From Fig. 6, the values of induced electromotive force are:

$$e= R_a.i + L_s\frac{di}{dt} + V \quad (10)$$

R_a: Armature resistance

L_s: Synchronous inductance

V: Voltage (V)

$$V= i.R_L \quad (11)$$

i: current (A)

The induced voltages in the windings for a single-phase are:

$$e_{ph} = K_E.\cos\left(\frac{\pi}{\tau}z\right).v(t) \quad (12)$$

z: Uniform variable displacement of the moving component

$$z = A.\sin\left(2.\pi.f.t - \frac{\pi}{2}\right) \quad (13)$$

A: displacement of the moving component

f: Movement frequency

v(t): Speed of the moving component

$$v(t)= z'= 2.\pi.A.f.\cos\left(2.\pi.f.t - \frac{\pi}{2}\right) \quad (14)$$

$$K_E = M_s .Ws. Nph. Φ. v_{av} \quad (15)$$

Differential equation for phase current

$$\frac{di}{dt} = \frac{e-v-i.Ra}{L_s} \quad (16)$$

The output power (P_{out}):

$$P_{out} = e_{ph}.i \quad (17)$$

The moving part displacement is equal to ±40mm at a maximum speed of 0.25 m/s and 0.5 m/s as in Fig. 7. At low speed, power generated by the PMLG is low due to displacement part motion is sinusoidal, so the generated voltage is almost sinusoidal. Current from 0.4 A increases to 1.8A as in Fig. 8, voltage increases from 3V to 12V as in Fig. 9, and power increases from 1.2 W to 15W as in Fig. 10. From

the simulation, speed increases from 0.25m/s to 0.5m/s although the increase is not significant, the transmitter power increased from 1.2W to 15W.

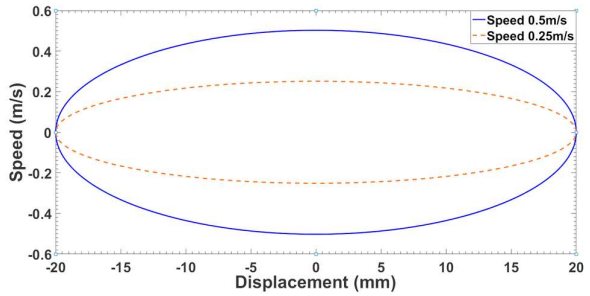

Fig. 7. Displacement of the moving component at a speed of 0.25 m/s and 0.5 m/s

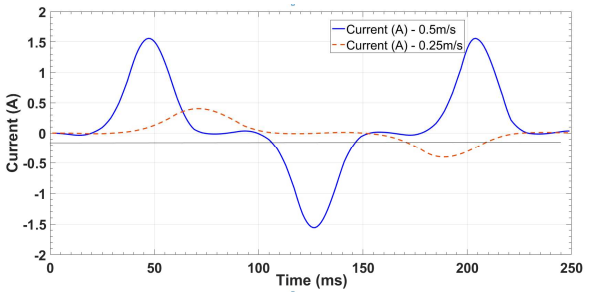

Fig. 8. Current (A) at maximum speed of 0.25 m/s and 0.5 m/s

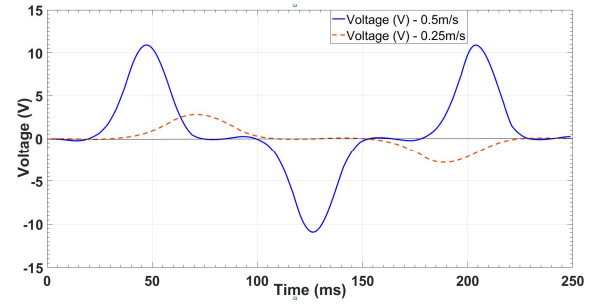

Fig. 9. Voltage (V) at maximum speed of 0.25 m/s and 0.5 m/s

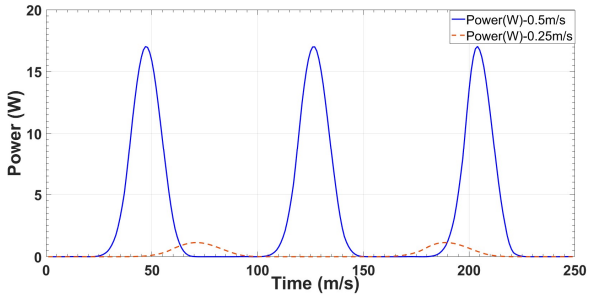

Fig. 10. Power (W) at maximum speed of 0.25 m/s and 0.5 m/s

III. Experimetnal Study

The simulation results provide important data to design an experimental model of PMLG as shown in Fig. 11. The linear motion of the moving component is generated by the 1.5HP motor through the eccentric gear mechanism and the speed is variable through the inverter. The experiment can be used pulse meter X431TOP with Channel: 4 CH; Maximum frequency of 20MHz; Measuring voltage of ±150V. It can be conducted in 2 cases: without and with a load of R_L=3.5Ω.

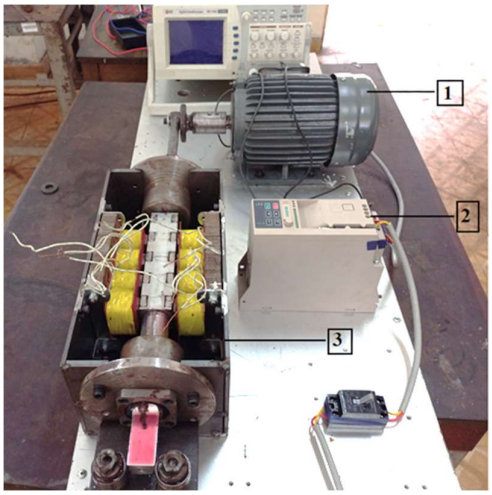

Fig. 11. Experimental model of PMLG; 1-Motor; 2-Inverter; 3-Linear Generator

Without a load of R_L, Fig. 12 shows an experimental speed of 0.25m/s (equivalent to 250ms per cycle), the achieved voltage is close to 20V. When the speed is increased to 0.5 m/s (equivalent to 150ms per cycle), the highest voltage is 40V as shown in Fig. 13.

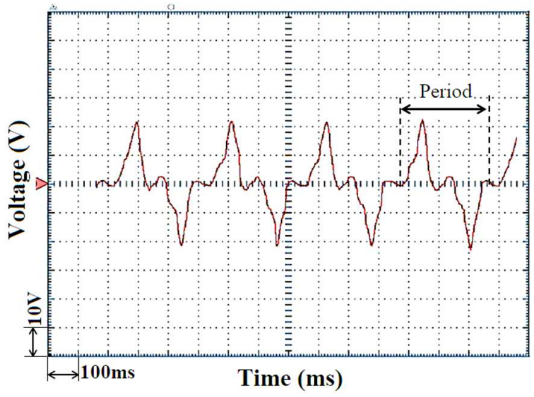

Fig. 12. Voltage at speed of 0.25 m/s without R_L

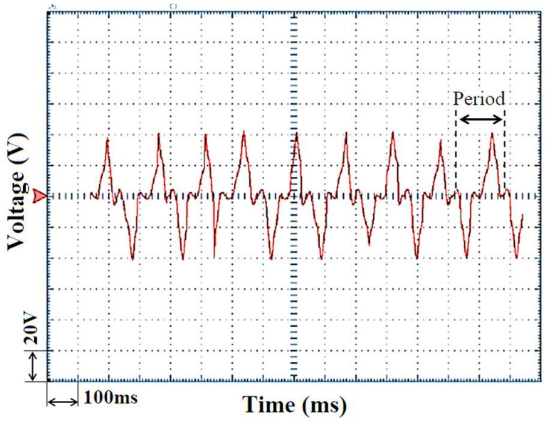

Fig. 13. Voltage at speed of 0.5 m/s without R_L

With a load of R_L=3.5Ω, Fig. 14 shows the experimental speed of 0.25m/s, the voltage achieved is close to 4V. When increasing the speed to 0.5 m/s, the peak voltage is 15V as shown in Fig. 15.

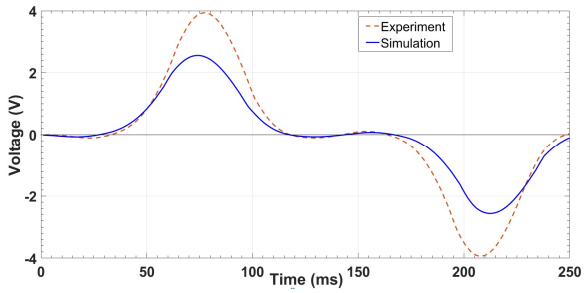

Fig. 14. Voltage at speed of 0.25 m/s with R_L=3.5Ω

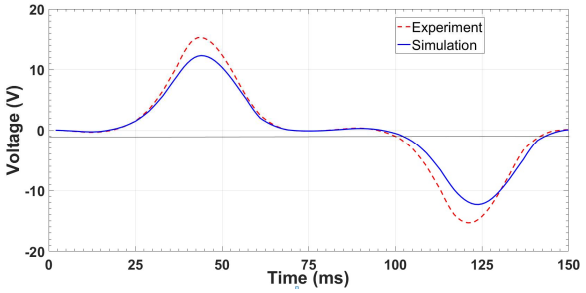

Fig. 15. Voltage at speed of 0.5 m/s with R_L=3.5Ω

Comparing the two experimental cases, the voltage drop is large with the load. The experimental speed can be adjusted to approximate the simulation speed, the comparison shows that the simulated voltage is less than the experimental one. The voltage difference due to the actual number of turns of the stator is different from the simulation model because of manual construction, and the experimental speed may be faster than the simulation speed due to the problem of inertial force control. In addition, the experimental model is more than the one that simulates a magnetic pole to supplement the magnetic field when the moving component reverses. The results demonstrate that the generator voltage can be predicted for different speeds. The waveforms from the oscilloscope are almost the same as the simulation results.

IV. Conclusion

By calculating, simulating parameters such as flux distribution density, inductance, etc. by using AM-V16 software and Matlab software to simulate power and current values for evaluating the characteristics of PMLG.

The simulation results showed that with a displacement of ±40mm when increasing the speed from 0.25m/s to 0.5m/s, the voltage increases from 3V to 12V, current from 0.4A to 1.8A, and power from 1.5W to15W. The simulation has been compared with the experimental results through the voltage parameter, when increasing the displacement speed from 0.25m/s to 0.5m/s the voltage increases 2 times (from 20V to 40V) without a load (R_L), and almost 4 times (from 4V to 15V) with a load of R_L=3.5Ω, respectively.

Acknowledgment

This work belongs to the project grant No: B2019-SPK-08 funded by Ministry of Education and Training, and hosted by Ho Chi Minh City University of Technology and Education, Vietnam.

References

[1] J. Zou, M. Zhao, Q. Wang, J. Zou, and G. Wu, “Development and analysis of tubular transverse flux machine with permanent magnet excitation,” IEEE Trans. Industrial Electronics, vol.59, no.5, pp.2198- 2207, May 2012.

[2] H. Jing, N. Maki, T. Ida, and M. Izumi, “Electromechanical design of an MW class wave energy converter with an HTS tubular linear generator,” IEEE Trans. Appl. Supercond., vol. 28, no. 4, Jun. 2018, Art. no. 4902504

[3] L. Huang, B. Hu, M. Hu, C. Liu, and H. Zhu, “Research on primary excitation fully superconducting linear generators for wave energy conversion,” IEEE Trans. Appl. Supercond., vol. 29, no. 5, Aug. 2019, Art. no. 5203405

[4] A. Gandhi and L. Parsa, “Thrust optimization of a five-phase faulttolerant flux-switching linear synchronous motor,” in Proc. IEEE Industrial Electronics Society Conf., pp.2067-2073, 2012.

[5] Hodgins, N.; Keysan, O.; McDonald, A.S.; Mueller, M.A. “Design and Testing of a Linear Generator for Wave-Energy Applications,”. IEEE Trans. Ind. Electron. 59, 2094–2103,201,.

[6] N. M. Kimoulakis, A. G. Kladas, and J. A. Tegopoulos. “Power Generation Optimization from Sea Waves by Using a Permanent Magnet Linear Generator Drive”. In: IEEE Transactions on Magnetics 44.6 (2008), pp. 1530– 1533.

[7] C. Liu, H. Yu, M. Hu, Q. Liu, S. Zhou, and L. Huang, “Research on a permanent magnet tubular linear generator for direct drive wave energy conversion,” IET Renewable Power Generation, vol. 8, no. 3, pp. 281–288, 2014.

[8] J. Hansson and M. Leksell., “Performance of a Series Hybrid Electric Vehicle with a Free-Piston Energy Converter,” IEEE Xplore, 2007.

[9] R. Mikalsen and A. P. Roskilly, “A review of free-piston engine history and applications,” Applied Thermal Engineering, vol. 27, pp. 2339- 2352, Oct 2007.

[10] B. Jia, R. Mikalsen, A. Smallbone, and A. Paul Roskilly, “A study and comparison of frictional losses in free-piston engine and crankshaft engines,” Applied Thermal Engineering, 2018.

[11] Ondřej Vysoký, “Linear combustion engine as main energy unit for hybrid vehicles,” Proceedings of Transtec Prague. Prague: Czech Technical University, 2007: p. 236-244.

[12] Ocktaeck Lim, Nguyen Ba Hung, Seokyoung Oh, Gangchul Kim, Hanho Song, Norimasa Iida, “A study of operating parameters on the linear spark ignition engine,”. Applied Energy, 2015. 160: p. 746-760.

[13] Subhash Nandkumar, Two-stroke linear engine. 1998, Dissertation, West Virginia University.

[14] R. Mikalsen and A. P. Roskilly, “The control of a free-piston engine generator. Part 2: Engine dynamics and piston motion control,” Applied Energy, vol. 87, 2010.

[15] Boru Jia, Zhengxing Zuo, Huihua Feng, Guohong Tian, A. P. Roskilly, “Development approach of a spark-ignited free-piston engine generator”. 2014, SAE Technical Paper, No. 2014-01-2894.

[16] F. W. Carter. “Air-Gap Induction”. In: Electric World and Engineer 38.22 (1901), pp. 884–888. url: http://hdl.handle.net/2027/uva.x030741299.

A Study of the Scavenging Process in a Two-stroke Free Piston Linear Engine at Low Velocity Using CFD and DPM

Nguyen Huynh Thi
Faculty of Vehicle and Energy Engineering,
Ho Chi Minh City University of Technology and Education
Ho Chi Minh City, Vietnam
nguyenhuynhthi@tgu.edu.vn

Nguyen Van Trang
Faculty of Vehicle and Energy Engineering,
Ho Chi Minh City University of Technology and Education
Ho Chi Minh City, Vietnam
trangnv@hcmute.edu.vn

Huynh Thanh Cong
Vietnam National University-Ho Chi Minh City
Ho Chi Minh City, Vietnam
htcong@hcmut.edu.vn

Dao Huu Huy
Faculty of Vehicle and Energy Engineering,
Ho Chi Minh City University of Technology and Education
Ho Chi Minh City, Vietnam
dhhuy2310@gmail.com

Huynh Van Loc
Faculty of Industrial Engineering, Tien Giang University
My Tho City, Vietnam

Truong Hoa Hiep
Faculty of Industrial Engineering, Tien Giang University
My Tho City, Vietnam

Ngo Duc Huy
Faculty of Vehicle and Energy Engineering,
Ho Chi Minh City University of Technology and Education
Ho Chi Minh City, Vietnam

Vo Bao Toan
Faculty of Vehicle and Energy Engineering,
Ho Chi Minh City University of Technology and Education
Ho Chi Minh City, Vietnam

***Abstract*—A free-piston linear engine (FPLE) does not use a crankshaft to control piston motion. The gas exchange and piston movement are closely related to each other and directly affecting to the engine performance. In this study, a numerical simulation using Computational Fluid Dynamics (CFD) and the Discrete Phase Model (DPM) has been performed to investigate the scavenging process in a two-stroke free piston linear engine during warm up. The characteristics of the reciprocating motion can be determined based on the dynamics model and the piston motion profiles are imported into commercial CFD software (Ansys Fluent V.21). Both models have been applied the initial conditions such as the velocity of the piston, piston displacement, and inlet pressure to assess the effect of the trapping efficiency. The results show that the trapping efficiency ±5% difference in two models that was able achieve at piston of 0.32 m/s – 1.25 m/s. In addition, the change in gas at each displacement position of the piston and different inlet pressures is also shown through the simulation results.**

***Keywords*— Free piston linear engine; scavenge efficiency; piston motion; Computational Fluid Dynamics (CFD); Discrete Phase Model (DPM).**

I. INTRODUCTION

The free-piston engine generator (FPLE) is a linear internal combustion engine that is removed the crank and piston move freely in the cylinder. With the advantages of compactness, high efficiency [1], variable compression ratio should be suitable for many different fuels [2], reducing friction compared to conventional heat engines [3]. Visibly, FPLE is a research trend to improve the performance of hybrid vehicles. The FPLE considered in the present research is the two-stroke dual-piston type. The piston assembly has a free linear motion between the top dead center (TDC) and bottoms dead center (BDC) and the piston assembly motion is controlled by gas and load forces acting upon it. Cancelling the crank mechanism allows the piston to move freely between the two cylinders, giving the engine the advantage of flexible characteristics, but also poses a challenge to the stability of the engine. The destabilization here is controlling the position of TDC before the combustion process; different positions of TDC produce different end-compression pressure that affects the power of the engine. There are so many related researches on the stability control of FPLE, and proposed various control methods [4-7]. These studies focus only on controlling the motion of the piston. Although considerable progress has been made, the way FPLE is controlled remains one of the problems preventing its commercialization. Another factor is the mass of air and fuel trapped inside the combustion chamber. The trapped mixtures are affected by the gas exchange process in there have scavenging process. That can be key to realizing the engine's combustion efficiency and emissions potential [8]. But the stability of gas exchange is unpredictable and difficult for measurement techniques.

CFD (Computational Fluid Dynamics) is a very useful tool to analyze the exchange gas through the motion process of FPLE as well as the scavenging process. Blarigan et al., at Sandia National Laboratories, studied the effects of design parameters such as gas pressure in box, inlet position, and tilt angle on scavenging efficiency and trapping efficiency of FPLE through CFD [9]. Their results indicate that during the early stages of gas exchange, some gas travels from the scavenging port to the exhaust port, causing direct trapping losses. Blarigan et al., at Sandia National Laboratories They introduced a non-dimensionally modeled piston movement configuration into the KIVA-3V, simulating it to obtain the basic FPLE scavenging performance with constant intake pressure using the model CFD [10]. The results show that a gas exchange system with continuously low rise pressure maximizes efficiency and reduces unclean emissions. In addition, several other studies show that FPLE has a faster piston speed than a conventional engine, which results in shorter gas exchange duration of FPLE, lower scavenge efficiency but higher trap efficiency [11-12].

The studies above show that the gas exchange process has been simulated and optimized the effects of design parameters to FPLE. However, these studies omitted the gas exchange in the start process of FPLE, this process usually operates at low speed but must ensure the trapping efficiency. This study presents a CFD simulation to investigate scavenging structure and parameters on the FPLE gas exchange process. The dimensional parameters are chosen based on a prototype FPLE, the motion of the free piston is built based on a dynamic model to calculate the piston's motion profiles. In this study, the key parameters such as displacement piston, operating low-frequency and inlet pressure are inlet parameters. Two methods CFD and the Eulerian-Lagrangian discrete phase model (DPM) is used to track the ratio of particles trapped and escape from the cylinder then find out trapping efficiency and compare the accuracy with each other.

II. MODELING AND SIMULSATION

A. Dynamic model

The mechanical forces acting on the piston include the gas force in the left and right cylinder, mechanical friction and inertia force, and traction of the actuator. Piston dynamics can be determined by Newton II's law.

$$F_{st} + F_{cyl} - F_{cyr} - F_f = m\frac{d^2x}{dt^2} \quad (1)$$

F_{cyl}, F_{cyr} are the gas force from the left and right cylinder

$$F_{cyl} = P_{cyl} \times S \quad (2)$$

$$F_{cyr} = P_{cyr} \times S \quad (3)$$

P_{cyl}, P_{cyr} is the pressure in the left and right cylinders; S is the area of the piston crown. F_f is the friction force, m is the mass of the translator, d^2x/dt^2 is the acceleration of the piston, F_{sl}, F_{sr} are respectively the spring forces in the left and right. F_{st} the force is received from the

starting device.

The velocity of piston is calculated by equation:

$$\frac{dx}{dt} = \left(\frac{dx}{dt}\right)_0 + \frac{d^2x}{dt^2}\, t \qquad (4)$$

On the actual model, the initial speed V_0 is based on the mechanical starter Fig 1 This speed is hindered by the spring forces in the left or right. The piston velocity of the BDC to TDC form is determined by:

$$V = V_0 - \frac{F.t}{m} \qquad (5)$$

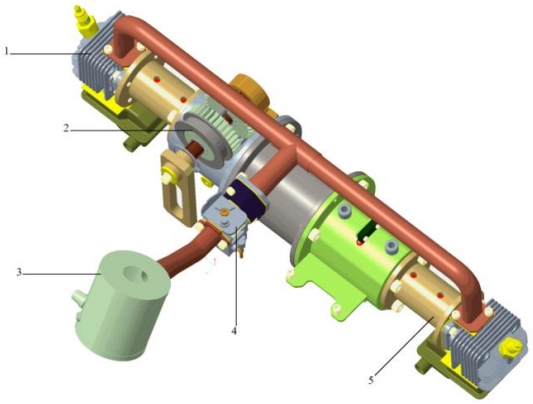

Fig. 1. A prototype of two-stroke free piston engine [15]

1- Cylinder 1; 2- Activation mechanism; 3- Compressor; 4-Carburetor, 5- Compressed air chamber; 6-Cylinder 2

B. CFD model

The piston model and main parameters of FPLE are shown in Fig 2 and Table 1. The parameter of the FPLE is imported into commercial CFD software Ansys Fluent v.21 to define the calculating surfaces and volumes as well as to generate the mesh. Then there is the meshing process, the cylinder mesh is generated in a multi-zone method, and the others have generated the mesh in the sweep method. The velocity of the piston is calculated by a program written in Microsoft Visual C++ before importing it into the Ansys software as an input database, the input database is a user-defined function (UDF). In the dynamic mesh, the layering is used to add or remove layers of cells according to the piston position. In addition, the dynamic mesh changes according to the piston position to change the compression ratio, pressure... The position of the piston can be changed step by step with a step of 0.5mm, from which it is possible to control the pressure at the end of the compression stroke in different locations.

In order to investigate the effects of intake pressure on the scavenging process and the pressure at the end compression, the inlet pressures are adjusted from 1.05bar to 1.2bar; initial speeds are 0.32m/s and 1.25m/s. The inlet and outlet temperatures are set at 300 K during the simulation process. The inlet mixture is assumed to be an ideal gas. In addition, the $k-\varepsilon$ turbulent model is employed to capture turbulence. Input parameters are provided for the computational fluid dynamic (CFD) model to calculate the trapping efficiency. In two-stroke, the trapping efficiency is defined as follows [13]:

$$\eta_t = \frac{\text{mass of delivered fresh charge retained in cylinder}}{\text{mass of delivered fresh charge through all scavenging ports}}$$

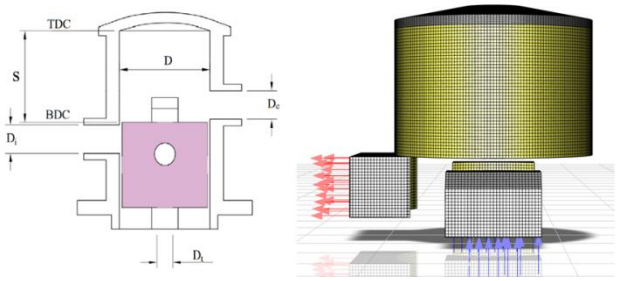

Fig 2. a) Parameter of the FPLE, b) Computational mesh of the FPLE

Table 1. ENGINE SPECIFICATIONS AND OPERATING CONDITIONS

Parameters	Values
Stroke (S)	28 mm
Bore (D)	34 mm
intake port d_i	0 - 6 mm
Exhaust port d_e	0 - 13mm
Transfer port D_t	10 mm
Inlet pressure Pin (bar)	1.05 - 1.25bar
Inlet temperature Tin (K)	300K

C. DPM model

The discrete Phase Model (DPM) is used to co track particles' motion. DPM is based on a Euler-Lagrangian framework, the forces such as viscous drag, lift force...acting on the particles along their trajectories and stochastic behaviour of the turbulent flow are taken into account. Based on tracking the particles throw discrete phases in boundary areas to escape, trap and reflect. Escape condition is assumed in the inlet and outlet ports, the trap condition is considered the cylinder and reflects condition is being a wall of intake and exhaust pipes Fig 3. To shorten the computational time and the approach become much simpler, assumptions in particle motion calculations will be simplified: all particles have the same size, and the flow around the particles and particle-particle interaction is neglected in the simulation. In the Lagrangian reference frame, the trajectory is predicted by integrating the force balance on each individual particle and can be written as [14]:

$$\frac{du_p}{dt} = \frac{u-u_p}{\tau_r} + \frac{g(\rho_p-\rho)}{\rho_p} + F \qquad (6)$$

where F is an additional acceleration (force/unit particle mass) term;ρ is the particle density and ρ_p is the continuum phase density; u is the local fluid phase velocity and u_p is the velocity of the particle phase, respectively; g is the gravity of the particle. The first

item on the right is the drag force per unit particle mass, τ_r is the droplet or particle relaxation time. The initial parameters of the particle such as velocity, mass flow inlet… similar to the CFD model; the trap efficiency in the DPM is replaced by the number of particles. The trapping efficiency is defined: as the number of particles entering the cylinder divided by the number of particles supplied from the scavenging ports.

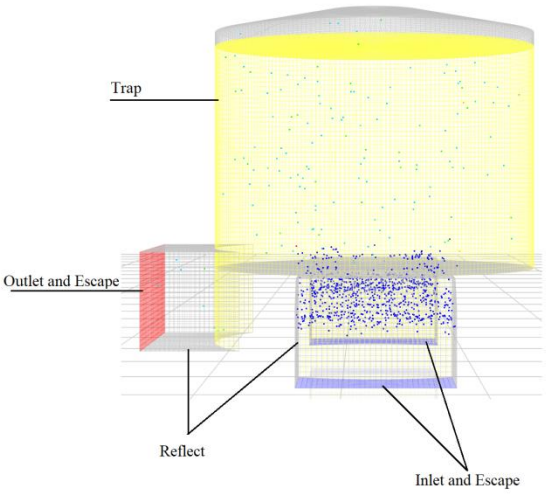

Fig 3. DPM calculation Model

III. RESULTS AND DISCUSSION

A. CFD simulation results

Pressure changes at the inlet port and open/closed position affect the scavenging process. At an initial speed of 0.32m/s, the initial pressure gradually increases from 1.05bar to 1.2bar. Trapping efficiency is increased but not significantly since the mass flow in/out of the cylinder is almost stable Fig 4. When the piston is close to fully closing the inlet, the mass flow drops suddenly at the 3.5 mm position and at the 4mm position the scavenge port fully close. At 1.05bar pressure due to high mass flow at the scavenge port but at the exhaust mass flow no significant difference with the case other so trapping efficiency still tends to increase; at 1.1bar pressure due to mass flow at the scavenge port low but high mass flow at exhaust port making the exhaust port high so trapping efficiency still tends to reduce. The flow velocity at the exhaust port is based on the flow velocity at inlet port, the flow velocity at the higher inlet the higher exhaust. The results of the flow velocity simulation De = 0mm; De =2mm; De =3.5mm at 1.05bar Fig 6 and the rest of the cases are shown in Fig7.

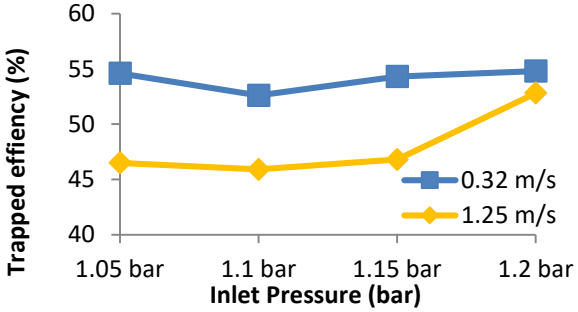

Fig 4. Trapping efficiency from 1.05bar to 1.25bar

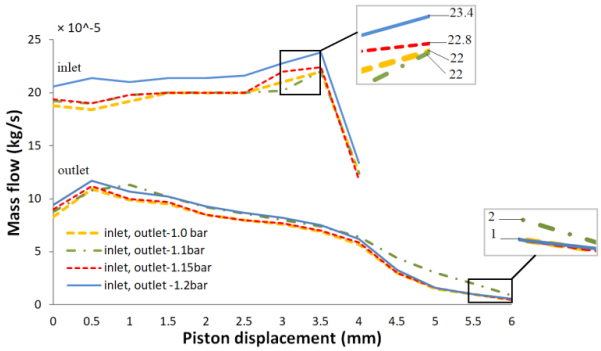

Fig 5. Mass flow versus piston displacement at piston speed 0.32m/s

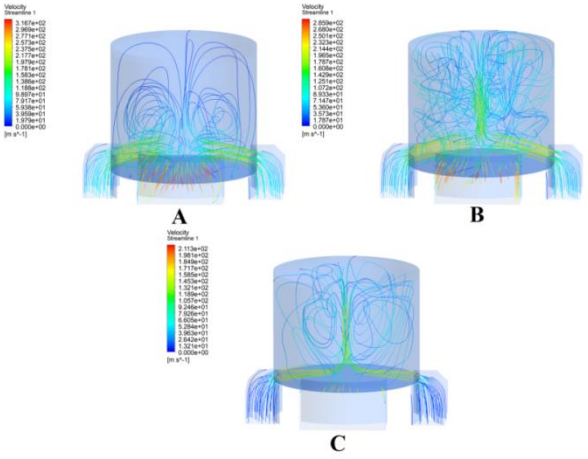

Fig 6. Velocity Streamline at A) D_e = 0mm; B) D_e = 2mm; C) D_e = 3.5mm with initial pressure = 1.05 bar and initial velocity of piston = 0.32m/s

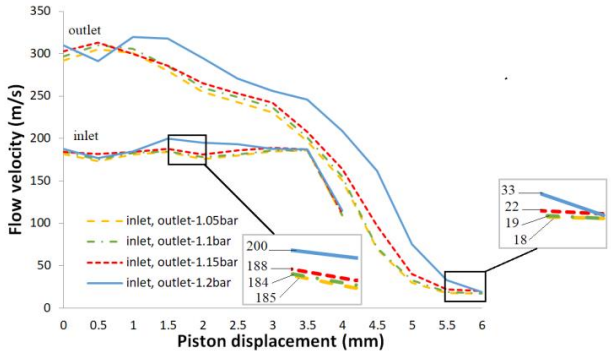

Fig 7. Flow velocity versus piston displacement at piston speed of 0.32m/s

When increasing the speed to 1.25m/s the trapping efficiency increases at 1.05bar pressure, more mass flows into the cylinder and out to the cylinder roughly equal to the other pressure curves. Through the two results, the speed of 0.32m/s still gives trapping efficiency higher than 1.25m/s, the reason is a lot of new charge going out of the exhaust port but new charge into cylinder low, as shown in the mass flow Fig 8 and the velocity simulation D_e = 0mm; D_e =2mm; D_e =3.5mm at 1.05bar Fig 9, the rest of the cases are shown in Fig 10.

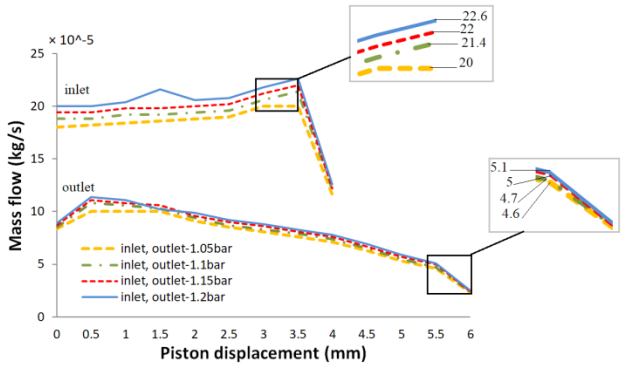

Fig 8. Mass flow versus piston displacement at piston speed 1.25m/s

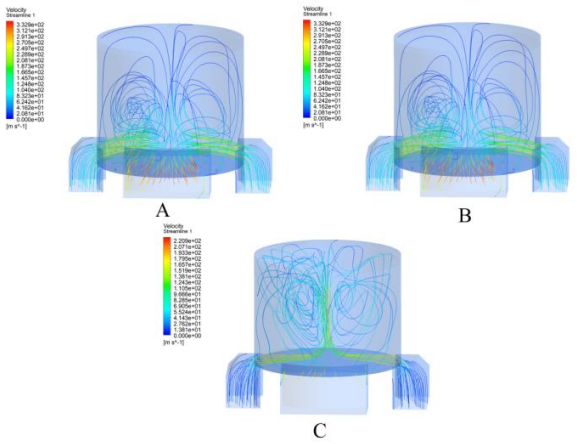

Fig 9. Velocity Streamline at A) D_e = 0mm; B) D_e = 2mm; C) D_e = 3.5mm with initial pressure = 1.05bar and initial velocity of piston = 1.25m/s

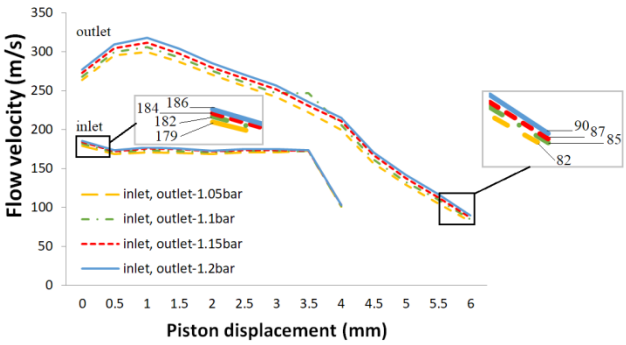

Fig 10. Flow velocity versus piston displacement at piston speed of 1.25m/s

B. DPM simulation results

With the same input conditions as the CFD model, the trapping performance has a difference in Fig 11, due to particle conditions such as the same size and collision between particles in this model. It is possible to observe the movement of particles and the number of particles trapped in the cylinder, the number of trapped particles corresponds to the amount that is lost through the exhaust port and trapped due to the obstruction of the piston wall at the scavenging ports Fig 12.

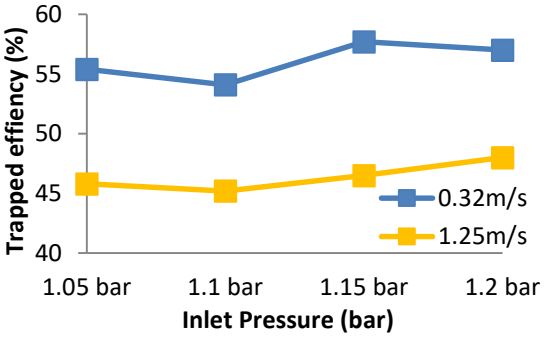

Fig 11. Trapping efficiency from 1.05 bar to 1.25 bar (DPM)

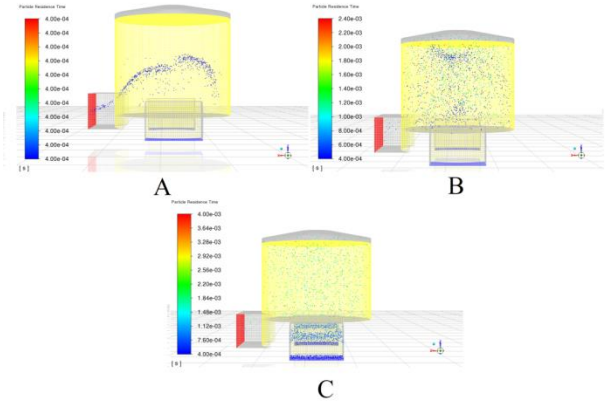

Fig. 12 A) Particle residence time at D_e = 0mm, B) Particle residence time at D_e = 4mm, C) Particle residence time at D_e = 6mm

With a low piston speed of 0.32m/s, the amount of particles trapped in the cylinder is high and stable. When the scavenging ports are completely closed, the number of trapped particles is reduced, causing large air escape through the exhaust port Fig 13. With a piston speed of 1.25m/s, the fast-closing time of the scavenging ports causes the number of particles not to catch up to the cylinder, but the number of particles retained is higher due to the fast-closing time of the exhaust port Fig 14. However, at 0.32m/s the trapping efficiency is still higher.

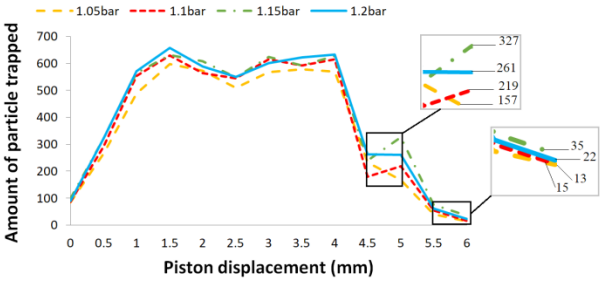

Fig 13. Amount of particle versus piston displacement at piston speed of 0.32m/s

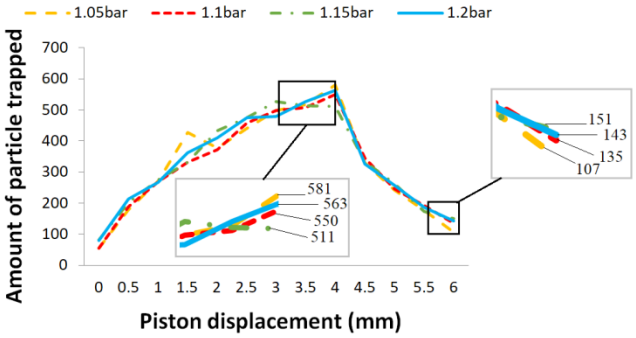

Fig 14. Amount of particle versus piston displacement at piston speed of 1.25m/s

IV. CONCLUSION

Based on the combination of the dynamic model, CFD model, and DPM model, the scavenging process in a two-stroke free-piston linear engine has been modelled and simulated. Although there is a ±5% difference in the trapping efficiency between the two models, there are still similarities in terms of rules. The influence of key parameters such as operating frequency, piston displacement changing intake/exhaust port, inlet pressure on scavenging and trapping efficiency were investigated. Simulation results show that the trapping efficiency is 0.32m/s higher than 1.25 m/s but not significant. Although the trapping efficiency at 1.25m/s speed is less than 0.32 m/s, there is still an advantage in terms of air loss between the piston and cylinder, which affects the starting process. In addition, simulation results also show that increasing exhaust port spacing, as well as reducing inlet pressure, can free the engine two-stroke piston to increase trapping efficiency. In the next works, velocity piston, and inlet pressure are changed more values to find the optimal parameters for the engine. In addition, the inlet temperature, the angle of inclination of the intake and exhaust manifolds and the geometry will be considered.

ACKNOWLEDGMENT

This work belongs to the project grant No: B2019-SPK-08 funded by Ministry of Education and Training, and hosted by Ho Chi Minh City University of Technology and Education, Vietnam.

REFERENCE

[1] J. Hansson and M. Leksell., “Performance of a Series Hybrid Electric Vehicle with a Free-Piston Energy Converter,” IEEE Xplore, 2007.

[2] R. Mikalsen and A. P. Roskilly, “A review of free-piston engine history and applications,” Applied Thermal Engineering, vol. 27, pp. 2339- 2352, Oct 2007.

[3] B. Jia, R. Mikalsen, A. Smallbone, and A. Paul Roskilly, “A study and comparison of frictional losses in free-piston engine and crankshaft engines,” Applied Thermal Engineering, 2018.

[4] R. Mikalsen, A.P. Roskilly, The control of a free-piston engine generator. Part 1: Fundamental analyses, Appl. Energy 87 (2010) 1273–1280.

[5] R. Mikalsen, A.P. Roskilly, The control of a free-piston engine generator. Part 2: Fig. 15. In-cylinder gas pressure and temperature of each combustion duration. C. Yuan, et al. Applied Thermal Engineering 173 (2020) 115201 10 Engine dynamics and piston motion control, Appl. Energy 87 (2010) 1281–1287.

[6] B.R. Jia, Z.X. Zuo, H.H. Feng, G.H. Tian, A. Smallbone, A.P. Roskilly, Effect of closed-loop controlled resonance based mechanism to start free piston engine generator: simulation and test results, Appl. Energy 164 (2016) 532–539.

[7] B.R. Jia, G.H. Tian, H.H. Feng, Z.X. Zuo, A.P. Roskilly, An experimental investigation into the starting process of free-piston engine generator, Appl. Energy 157 (2015) 798–804.

[8] Goldsborough SS, Blarigan P V. Optimizing the scavenging system for a two-stroke cycle, free piston engine for high efficiency and low emission: A computational approach. SAE Paper 2003-01-0001, 2003.

[9] A. Sofianopoulos, Y.C. Zhou, B. Lawler, S. Mamalis, Gas exchange processes of a small HCCI free piston engine - A computational study, Appl. Therm. Eng. 127 (2017) 1582–1597.

[10] S. Goldsborough, P. Blarigan, Optimizing the scavenging system for a two-stroke cycle, free-piston engine for high efficiency and low emissions: a computational approach, SAE Paper, No.2003-01-0001, 2008.

[11] C. Yuan, H. Ren, X. Jing, Comparison of the gas exchange of a loop scavenged freepiston engine alternator and the conventional engine, Appl. Therm. Eng. 127 (2017) 638–649.

[12] Nguyen Ba Hung, Sung Jaewon, Ocktaeck Lim. (2017). A study of a scavenging process in a two-stroke free piston linear engine using CFD. 9th International Conference on Applied Energy (pp. 1354-1360). Cardiff, UK: Elsevier Ltd.

[13] Grljuši´c, M.; Tolj, I.; Radica, G.; Sciubba, E. An Investigation of the Composition of the Flow in and out of a Two-Stroke Diesel Engine and Air Consumption Ratio. Energies 2017, 10, 1.

[14] A. Vakhrushev, M. Wu, A. Ludwig, G. Nitzl, Y. Tang, & G. Hackl, “Verification of a Discrete Phase Model with Water-Particle Flow Experiments in a Tundish,” in 5th. Int. Conf. on Simulation; Modeling of Metall, Processes in Steelmaking (STEELSIM) (2013).

[15] N. H. Thi et al., "An Investigation on Power Generation Characteristics of Linear Generator Driven by a Free-piston Engine," 2021 International Conference on System Science and Engineering (ICSSE), 2021, pp. 495-499, doi: 10.1109/ICSSE52999.2021.9538476.

JTE HCMUTE
ISSN: 2615-9740

JOURNAL OF TECHNICAL EDUCATION SCIENCE
Ho Chi Minh City University of Technology and Education
Website: https://jte.hcmute.edu.vn/index.php/jte/index
Email: jte@hcmute.edu.vn

A Preliminary Study of Spark-Ignition System for Free-Piston Linear Engine

Van-Trang Nguyen[1*], Huynh-Thi Nguyen[1], Thanh-Cong Huynh[2], Huu-Huy Dao[1]

[1]*Faculty of Vehicle and Energy Engineering, Ho Chi Minh City University of Technology and Education, Ho Chi Minh City, Vietnam*
[2] *Vietnam National University-Ho Chi Minh City Ho Chi Minh City, Vietnam*

[*] Corresponding author. *Email:* trangnv@hcmute.edu.vn

ARTICLE INFO

Received: 18/09/2022
Revised: 24/10/2022
Accepted: 01/11/2022
Published: 28/02/2023

KEYWORDS

Free-piston engine;
Internal combustion engine;
Linear generator;
Ignition system;
Starting system.

ABSTRACT

In recent years, the free-piston linear engine (FPLE) has attracted increasing interest from researchers worldwide. With the development of computer control technology, internal combustion engine technology, and material science, there have been significant advances in the aspects of FPLE simulation, experimental techniques, as well as systems FPLE control. This paper presents a model of a two-stroke, spark-ignition free-piston engine converted from two small two-stroke engines. It has a bore size of 34 mm and a maximum stroke of 28 mm. The linear engine uses gasoline fuel that is available on the market. The purposes of the research show a model of the starting system, investigation the effects of spark timing, and effective pressure. A premixed air-fuel charge is conducted by a carburetor then it is directly supplied into each cylinder. The spark timing was varied at 1 mm and 2 mm away from the maximum top dead center with the speed starting at 10 Hz. The model successfully ignited with a maximum pressure of 7.5 kg/cm^2 at the ignition of 1 mm before top dead center (TDC) and 9.5 kg/cm^2 at the ignition of 2 mm before TDC. The research has completed the initial intentions such as a theoretical investigation, calculation, determination of the engine model, and starting mechanism. Preliminary results have confirmed the feasibility of proposing the FPLE model.

Doi: https://doi.org/10.54644/jte.75A.2023.1281

1. Introduction

Linear engines aren't a new idea, it is first proposed in the early 1920s [1]. However, compared to conventional internal combustion engines; it is unnoticed because of some issues such as control, application... In recent years, due to environmental pollution and energy issues, research on alternative high-efficiency internal combustion engines is considered to be one of the most attractive research topics. Outstanding among them is a linear engine because the linear engine removed the crankshaft mechanism, which allows the piston to move freely inside the cylinder liner. This helps the engine reduce mechanical friction losses and variegates compression ratios under different load conditions, and fuel types [2-3]. Besides, researchers have started investigating it as a generator using a linear alternator used as an auxiliary power source in a hybrid.

Unlike traditional internal combustion engines, the lack of a crankshaft and a flywheel mechanism makes a linear engine not have a fixed rotation angle. Therefore, the control of top dead center (TDC) becomes complicated with a small deviation leading to the dynamics of the piston instability. The dynamics of the piston are determined by the resultant forces applied, such as the in-cylinder peak pressure, the electric load force, and the friction. In dual-piston linear 2 engines, TDC is considered the piston point of reverse movement. Thus, TDC in the current cycle depends on the previous cycle. In this model, the electric load force is removed. Therefore, the in-cylinder peak pressure is an important parameter to control the engine. The in-cylinder peak pressure is too high or low in this cycle will affect the load, and speed of piston movement in the cycle opposite. Similarly in engine 2, spark ignition, spark timing is an important factor affecting the formation of peak pressure in a cylinder [4-7]. Besides, a parameter considered is the initial compression pressure, high compression pressure and high density of air in the combustion chamber leading to short burning time, the peak

JTE
HCMUTE
ISSN: 2615-9740

JOURNAL OF TECHNICAL EDUCATION SCIENCE
Ho Chi Minh City University of Technology and Education
Website: https://jte.hcmute.edu.vn/index.php/jte/index
Email: jte@hcmute.edu.vn

pressure is formed earlier than expected. At present, the optimal controller for two-piston configuration linear motors is still the large challenge, although there are many research groups in this field through simulation or experimentation [8-11]. Some simulations focus on finding connections between kinetic influencing factors but still encounter difficulties in certain issues. Several studies have shown that a variety of factors affecting combustion and dynamics are needed to increase the stability of linear engines based experiments conducted [12-14].

In this paper, the ignition timing affects the FPLE combustion mentioned with the speed slow of the piston at a linear frequency 10Hz. A dual linear design was introduced, to simplify the dynamic factors so the generator was removed, instead of a mechanical starter system. The carburetor with high pressure is entered into the cylinder via a compressor. The effect of spark time, piston startup speed, pressure at ignition time, and ignition time are studied based on simulation. The simulation was performed with commercial software, MATLAB / SIMULINK, a designed model based on a Wiebe function used to simulate the combustion process. The resulting simulation will be the basis for the experiment conducted to consider the starting ability.

2. Development of Engine Model

The model is shown in figure 1, two engines and two-stroke forced ignition are placed at both ends. Friction between parts has minimum friction due to lubrication. A carburetor is used to distribute it before putting it into the cylinder. Varying the velocity of the airflow helps the pressure difference enter the carburetor and the nozzle of the nozzle. When opening the air inlet, it is put into the compressed air chamber and then compressed into the combustion chamber through the transfer port. A locking mechanism that locks the piston does not exceed the desired point - the top dead center.

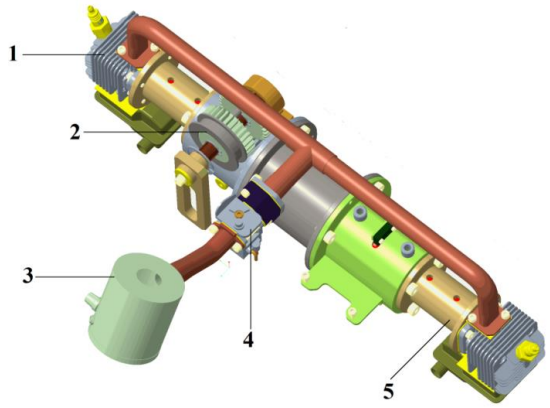

Figure 1. *A 3D model of two-stroke free piston engine*

1- Cylinder; 2- Starter mechanism; 3- Compressor; 4-Carburetor, 5- Compressed air chamber

Principle of operation, Stages first: the intake air is brought into the intake port by the compressor, and the air stream passes through the carburetor where the gas is mixed with the fuel. Then the mixture enters the compressed air chamber and the combustion chamber via the transfer port, and the compression stroke begins when the exhaust port and the transfer port close. Stages second: When the piston is on the TDC, the spark plug creates a high pressure that pushes the piston in the opposite direction and opens the valve, bringing the gas out of the cylinder.

A separate mechanical start-up system is presented, the failure to integrate the starter and separate it from the transmitter will help reduce the cross-section, and the weight of the transmitter, and reduce the complexity of control. However, it increases the shaft length and the mass of the shaft. Like a conventional engine at start-up, the linear engine must be set to a certain frequency to produce the necessary compression pressure by mechanical resonance [15]. The goal of the starter system in this design is to convert from rotary motion to linear motion. The conversion is made by a gear structure, which is shown in figure 2. The speed sensors located in the sensor chamber will check the motor speed, piston movement speed, and ignition position. When the engine starts successfully, the mechatronic mechanism will remove the gear from the gear bar when the piston moves freely in the cylinder.

JTE
HCMUTE
ISSN: 2615-9740

JOURNAL OF TECHNICAL EDUCATION SCIENCE
Ho Chi Minh City University of Technology and Education
Website: https://jte.hcmute.edu.vn/index.php/jte/index
Email: jte@hcmute.edu.vn

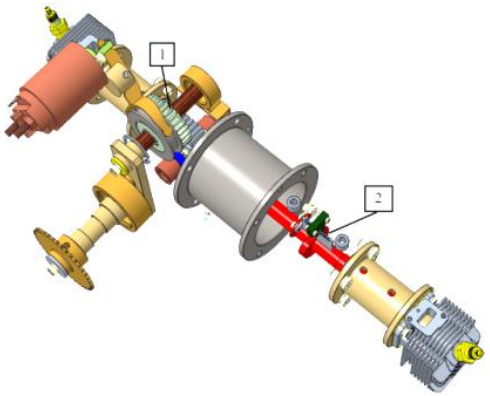

Figure 2. *Mechanical start-up of FPLE*

1- The starter mechanism; 2- The sensor chamber

3. Conceptual Design of the Ignition System

3.1. Design of Ignition System

In this model, the ignition system is no different from a conventional engine. The spark of ignition system is created from the 12V battery, ignition coil, control system, and spark plug. The model uses a transistorized ignition system (TI), with simple control advantages. Ignition signals are generated by a control program with signals based on position sensor, ignition time before TDC. The structure of the position sensor consists of an optical sensor and a gear bar with 1mm spacing that determine the position and movement. Based on, the signal from the position sensor, the ignition time before 1mm, 2mm before TDC, was chosen as the early ignition time for experimental simulation. The 5v signal generated using the primary control coil of the ignition coil will trigger a voltage of more than 30 kV in the secondary coil of the ignition coil. High voltage is transmitted to the spark plug electrode to ignite and ignite the charge in the cylinder. The ignition strategy is shown in Figure 3 and Control system diagram shows in Figure 4.

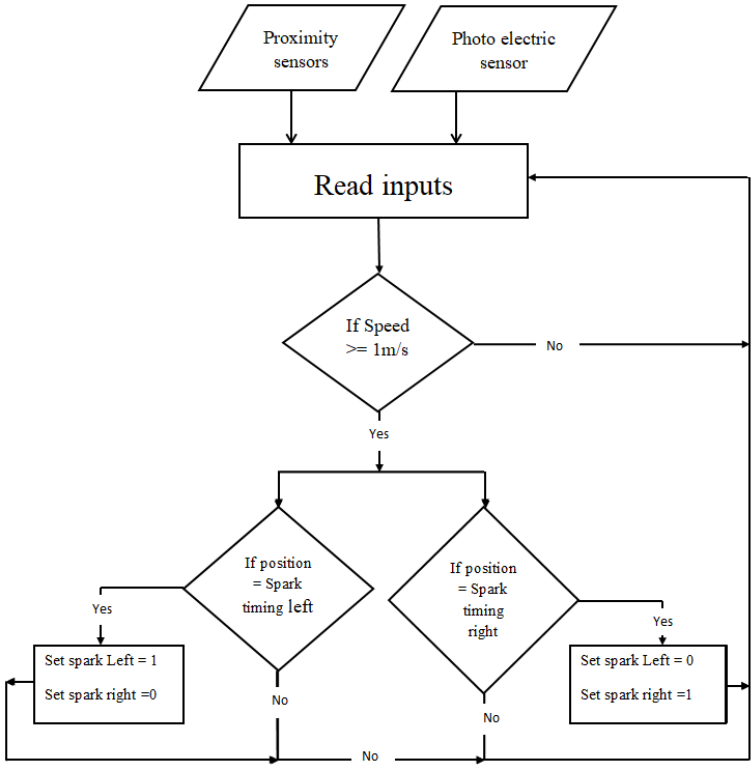

Figure 3. *The ignition control strategy*

JTE
HCMUTE
ISSN: 2615-9740

JOURNAL OF TECHNICAL EDUCATION SCIENCE
Ho Chi Minh City University of Technology and Education
Website: https://jte.hcmute.edu.vn/index.php/jte/index
Email: jte@hcmute.edu.vn

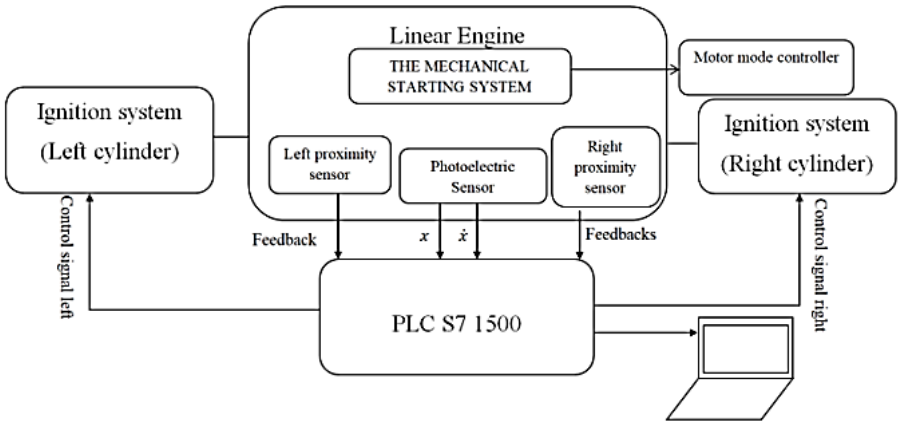

Figure 4. *Control system diagram*

3.2. Simulation

The simulation parameters of the model are shown in Table 1.

Table 1. *Free-piston engine specifications*

Description	Specification
Number of cylinder	2
Engine type	2 stroke
Bore	34 mm
Stroke	28 mm
Moving mass	0.58 kg
Nominal compression ratio	7.5:1
Fuel type	gasoline

The free-piston engine model is separated into a combustion chamber model to set initial parameter conditions such as piston displacement speed, ignition time, and compression pressure. Initial piston speed determined by the pull of the starter system, the previous combustion takes place after successful ignition.

Application in cylinders can be assessed by the derivative form of the first law of thermodynamics. The simulation will be based on Matlab/Simulinks software.

$$\frac{dy}{dx} = -\gamma.\frac{p}{V}.\frac{dV}{dt} + (\gamma - 1)\frac{Q_{in}}{V}\frac{dx_b}{dt} \quad (1)$$

P is in-cylinder pressure (MPa); γ is the specific heat ratio; V is in-cylinder volume (m^3); Q_{in} is the input heat energy; x_b is mass fraction burned (MFB). The combustion process, which simulates the mass fraction burned, is performed by the Wiebe function [16,17].

$$x_b = 1 - \exp\left[-a\,.\,\left(\frac{t - t_s}{C_d}\right)^{b+1}\right] \quad (2)$$

C_d: is the combustion duration; t_s: is time to start ignition. The constants of a = 5 and b = 2 are used. These constants are widely used for general ignition engines and it has been shown that they correlate well with experimental data [18].

Initial experiments shown that the pressure at the start of the ignition is about 4.5 MPa at 1 mm and 2 mm BTDC with an engine speed of 10 Hz, this is the goal to be achieved for the ignition process to succeed. Simulated burning time ($t-t_s$) 5 ms, 10 ms, 15 ms, and 20 ms with 100% mass fraction burned.

JTE
HCMUTE
ISSN: 2615-9740

JOURNAL OF TECHNICAL EDUCATION SCIENCE
Ho Chi Minh City University of Technology and Education
Website: https://jte.hcmute.edu.vn/index.php/jte/index
Email: jte@hcmute.edu.vn

It is assumed that the peak pressure is the pressure value that pushes the piston in the opposite direction. Therefore, the peak pressure must be released before the piston impacts with the top of the cylinder. In this simulation, TDC is the limit of displacement between the rack and pinion gears. The simulation in Figure 5 and Figure 6 shows a start speed of 10 Hz and successful ignition at 1 mm and 2 mm BTDC. At 2 mm BTDC is the best ignition timing because peak pressure is almost located at TDC. The peak pressure decreases when the burning time is long because most of the fuel burns when the starting device brings down the piston.

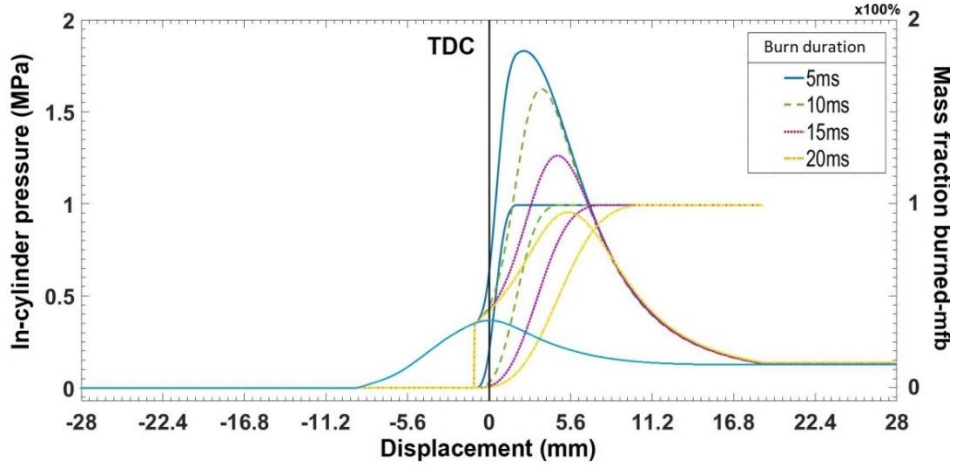

Figure 5. *The peak pressure at piston position of 1 mm BTDC*

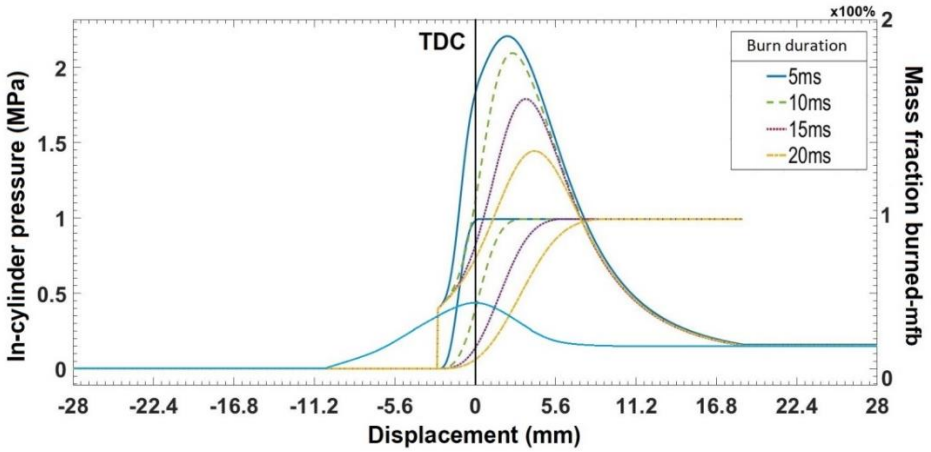

Figure 6. *The peak pressure at piston position of 2 mm BTDC*

In FPLE, the successful ignition of the first cylinder has influence on the opposite one, the raise of in-cylinder pressure resulted the increase of piston acceleration. If the ignition timing of the opposite cylinder is not changed, the engine will become unstable and collide with the peak cylinder. The impact of the piston on the blocking mechanism will suppress the inertial force so that the compression ratio is stable, reducing the possibility of fire loss, but the engine will not operate smoothly. In fact, FPLE does not need to form the maximum pressure, just a force greater than the pressure from the ignition pressure of the opposite cylinder, the piston can move backwards. Therefore, the appropriateness of the ignition timing is the decisive factor for the stable operation of the FPLE.

4. Results and Discussion

The experimental model of the mechanical starting system is shown in Figure 7. The data of piston displacement and piston velocity is measured through a photoelectric sensor Omron EE-SX670A and position sensor plate, the resolution of sensors 1 mm as show in Figure 4. The displacement direction

JTE
HCMUTE
ISSN: 2615-9740

JOURNAL OF TECHNICAL EDUCATION SCIENCE
Ho Chi Minh City University of Technology and Education
Website: https://jte.hcmute.edu.vn/index.php/jte/index
Email: jte@hcmute.edu.vn

uses 2 proximity sensors Hanyoung UP08RD-2PA for two-way displacement left and right. In-cylinder gas pressure is measured by the Sensys M5256 pressure sensor, the sensor is able to measure from 0 MPa to 3 MPa and it corresponds to the voltage range 0V to 5V. The data generated from the sensors is acquired by a PLC s7 1500 and synchronized with the real time.

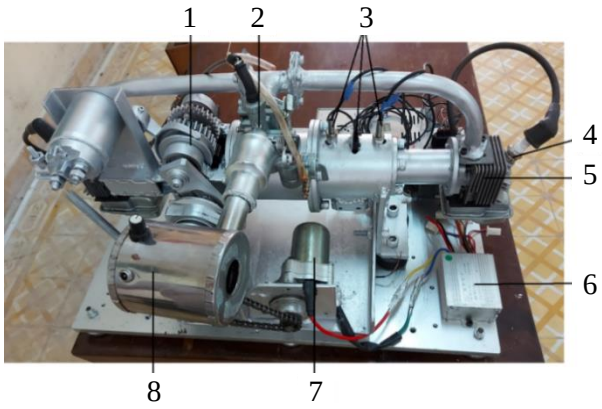

Figure 7. *Experimental model of PFLE*
1- Activation mechanism; 2-Carburetor; 3- Sensors; 4- Ignition system 5- Cylinder; 6-Motor mode controller; 7- Motor ; 8- Compressor

Figure 8 shows the maximum speed that can achieve 1 m/s equivalent to a frequency of about 10 Hz. The speed can be changed by changing the mode motor controller, however too high engine speed increases the force of inertia, affecting the airflow into the cylinder.

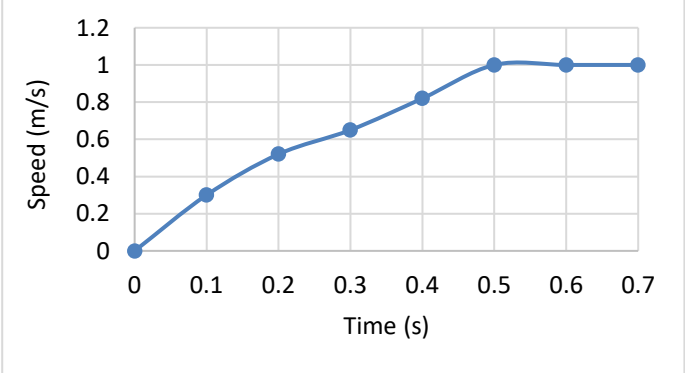

Figure 8. *Piston speed versus starting time*

In about 2 seconds, the maximum pressure reached 4.5 kg/cm^2 shown in Figure 9. Similar to other studies [19-21], the pressure in the cylinder to reach the maximum must have a certain number of oscillations. The maximum pressure between cylinder 1 and cylinder 2 is approximately the same, the maximum pressure in cylinder 1 reached 4.5 kg/cm^2 faster than in cylinder 2.

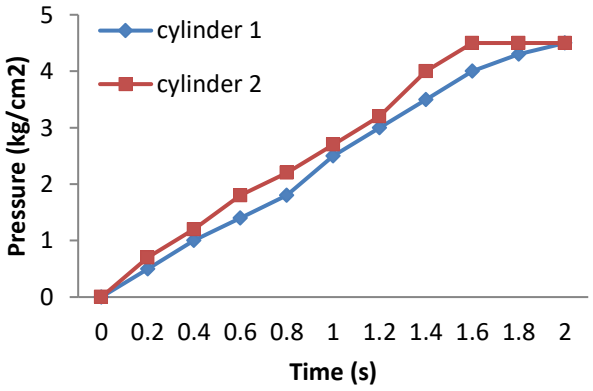

Figure 9. *Compression pressure in the cylinder and starting time*

JTE
HCMUTE
ISSN: 2615-9740

JOURNAL OF TECHNICAL EDUCATION SCIENCE
Ho Chi Minh City University of Technology and Education
Website: https://jte.hcmute.edu.vn/index.php/jte/index
Email: jte@hcmute.edu.vn

Figure 10, and Figure 11 show the engine model has successfully started up. With the speed engine of 10 Hz, the maximum pressure when successful ignition reaches over 7.5 kg/cm^2 at the ignition of 1 mm BTDC and 9.5 kg/cm^2 at the ignition of 2 mm BTDC when the starting system is still working.

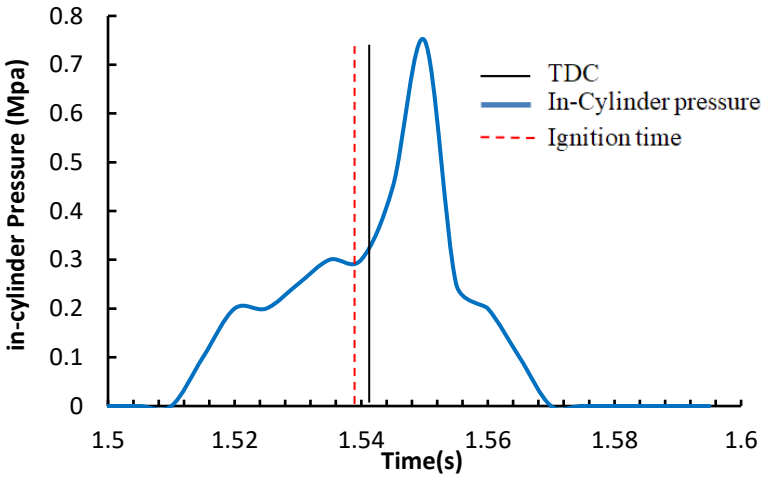

Figure 10. *Peak pressure for successful startup at 1 mm BTDC*

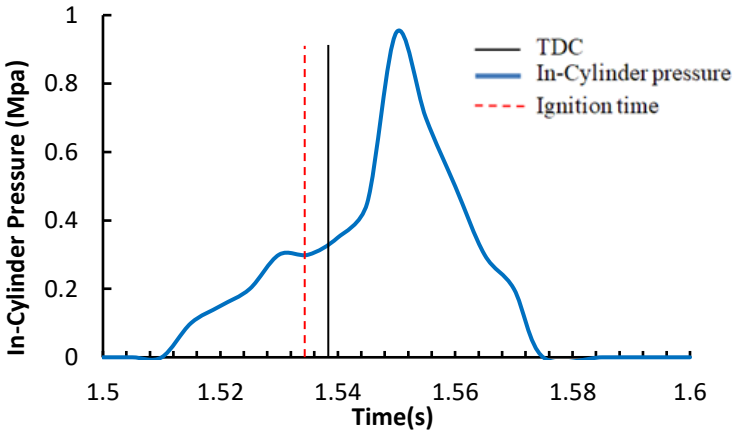

Figure.11. *Peak pressure for successful startup at 2 mm BTDC*

There is a no larger difference between the time of peak pressure formation. The engine misfire problem occurred quite a lot in the next ignition. There are many parameters affecting the ignition success such as the friction, injection time, and airflow into the cylinder. This study focused on the influence of ignition time on combustion, it can be seen that 2 mm pre-ignition timing before TDC will give higher peak pressure.

5. Conclusions

This paper presented a model of a two-stroke, spark-ignition free-piston engine converted from two small two-stroke engines. It has a piston with a 34 mm diameter and a maximum stroke of 28 mm. The spark timing was varied at 1 mm and 2 mm away from top dead center while the speed starting was varied at 10 Hz. The research showed that FPLE ignition was successful and reached over 7.5 kg/cm^2 and 9.5 kg/cm^2. The FPLE model has not yet reached a steady state caused by problems with ignition control, pressure and effect of the opposite cylinder. However, the results of this study may help the additional work for making the FPLE.

Acknowledgments

This work belongs to the project grant No: B2019-SPK-08 funded by Ministry of Education and Training, and hosted by Ho Chi Minh City University of Technology and Education, Vietnam.

REFERENCES

[1] Pescara, R.P., "Motor compressor apparatus", US patent 1,657,641, 1928.
[2] Mikalsen R, Roskilly AP. "A review of free-piston engine history and application". Apply Thermal Engineering 2007; 27:2339–52.
[3] Mao J L, Zuo Z X, Li W, Feng H. "Multi-dimensional scavenging analysis of a free-piston linear alternator based on numerical simulation". Applied Energy, vol.88, 2011.
[4] Huang L. "An opposed-piston free-piston linear generator development for HEV". SAE paper 2012-01-1021; 2012.
[5] L. Tunka and A. Polcar, "Effect of Various Ignition Timings on Combustion Process and Performance of Gasoline Engine," Acta Universitatis Agriculturae et Silviculturae Mendelianae Brunensis, vol. 65, no. 2, pp. 545-554, 2017.
[6] B.R. Jia, G.H. Tian, H.H. Feng, Z.X. Zuo, A.P. Roskilly."An experimental investigation into the starting process of free-piston engine generator". Appl. Energy157, 798–804, 2015.
[7] J. Kim, C. Bae, and G. Kim, "Simulation on the effect of the combustion parameters on the piston dynamics and engine performance using the Wiebe function in a free piston engine," Applied Energy, vol. 107, pp. 446-455, 2013.
[8] O. Lim and N. B. Hung, "A study of operating parameters on the linear spark ignition engine", Applied Energy, 746-760, 2015.
[9] [Feng Huihua, Guo Chendong, Jia Boru, Zuo Zhengxing, Guo Yuyao, Roskilly Tony. "Research on the intermediate process of a free-piston linear generator from cold start-up to stable operation: Numerical model and experimental results". Energy Convers Manage 2016; 122:153–64.
[10] Hung, N.B., Lim, O.T. "A study of a two-stroke free piston linear engine using numerical analysis". J Mech Sci Technol 28, 1545–1557 2014.
[11] Oh Y, Lim O. "A study for generating power on operating parameters of power pack utilizing linear engine". SAE paper 2012-32-0061; 2012.
[12] Kim J, Bae C, Kim G. "Simulation on the effect of the combustion parameters on the piston dynamics and engine performance using the Wiebe function in a free piston engine". Appl Energy 2013; 107:446–55.
[13] Mohd Razali Hanipah, "Development of a spark ignition free-piston engine generator". Dissertation, Newcastle University, 2015.
[14] Jia B, Tian G, Feng H, Zuo Z, Roskilly AP. "An experimental investigation into the starting process of free-piston engine generator". Appl Energy 2015; 157: 798–804.
[15] R. Mikalsen and A. P. Roskilly, "The control of a free-piston engine generator. Part 2: Engine dynamics and piston motion control," Applied Energy, pp. 1281-1287, 2010.
[16] J. B. Heywood, Internal combustion engine fundamentals, McGrawHill Book Company, New York, USA 2018.
[17] Fredriksson J, Bergman M, Golovitchev V, Denbratt I. "Modeling the effect of injection schedule change on free piston engine operation," SAE paper 2006-01- 0449; 2006.
[18] Yitong Jiang a, Daojing Wang, Fushui Liu, Shuwei Zhao, and Qing Yang. "Dynamic Simulation of a Two-Stroke Spark Ignition Free Piston Engine Generator". pp 225-230. 2014.
[19] R. Mikalsen, E. Jones, and A. P. Roskilly, "Predictive piston motion control in a free-piston internal combustion engine," Applied Energy, vol. 87, pp. 1722-1728, 2010.
[20] N. H. Thi et al., "An Investigation on Power Generation Characteristics of Linear Generator Driven by a Free-piston Engine", 2021 International Conference on System Science and Engineering (ICSSE), 2021, pp. 495-499.
[21] N. H. Thi, N. V. Trang, H. T. Cong, H. V. Loc, D. H. Huy and N. D. Huy, "A Preliminary Study of a Two Stroke Free-Piston Engine for Electricity Generation", 2020, 5th International Conference on Green Technology and Sustainable Development (GTSD), 2020, pp. 669-672.

Van-Trang Nguyen received his B.S. in Mechanical Engineering from Vietnam National University, Ho Chi Minh City University of Technology in 2002 and M.S. degrees from Ho Chi Minh City University of Technical Education (HCM UTE) in 2004 respectively. He then received his Ph.D degree from Yeungnam University, Republic of Korea, in 2014. He is currently a lecturer at the Ho Chi Minh City University of Technology and Education, Vietnam. His research interests focus on internal combustion engine, electric vehicle, and mechanical vibration.

Huynh-Thi Nguyen received the B.Eng and Master of Engineering in Faculty of Vehicle and Energy Engineering, in 2001 and 2006 respectively. He is a Ph.D student at Faculty of Vehicle and Energy Engineering in Ho Chi Minh City University of Technology and Education, Viet Nam.
Currently, his research interests include the Magnet Linear Generator and free-piston internal combustion engine.

Thanh-Cong Huynh received his B.S. degrees in Mechanical Engineering from Ho Chi Minh City University of Technology, Vietnam, in 2000. He received M.S degree in Thermal and Energy Engineering in L'Ecole Centrale de Lyon, France, in 2004. He received his Ph.D. degree in Thermal and Fluid Engineering in School of Mechanical Engineering (special in internal combustion engine), Sungkyunkwan University, Republic of Korea, in 2009. He has currently served as a Deputy Director of Department of Science and Technology, Vietnam National University – Ho Chi Minh City. Dr. Cong's research interests include: next generation of internal combustion engines with higher thermal efficiency (free-piston, gas engines,...), electric vehicles...

Huu-Huy Dao received B.Eng and M.Eng in Faculty of Vehicle and Energy Engineering at Ho Chi Minh City University of Technology and Education, Viet Nam.
His research interests include the Magnet Linear Generator and free-piston internal combustion engine.

Metadata of the chapter that will be visualized in SpringerLink

Book Title	From Smart City to Smart Factory for Sustainable Future: Conceptual Framework, Scenarios, and Multidiscipline Perspectives	
Series Title		
Chapter Title	Preliminary Design of a Single-Phase Linear Generator for Free-Piston Engine Application	
Copyright Year	2024	
Copyright HolderName	The Author(s), under exclusive license to Springer Nature Switzerland AG	
Author	Family Name	**Thi**
	Particle	
	Given Name	**Nguyen Huynh**
	Prefix	
	Suffix	
	Role	
	Division	
	Organization	Ho Chi Minh City University of Technology and Education
	Address	Ho Chi Minh City, Vietnam
	Email	
Corresponding Author	Family Name	**Trang**
	Particle	**Van**
	Given Name	**Nguyen**
	Prefix	
	Suffix	
	Role	
	Division	
	Organization	Ho Chi Minh City University of Technology and Education
	Address	Ho Chi Minh City, Vietnam
	Email	trangnv@hcmute.edu.vn
Author	Family Name	**Cong**
	Particle	
	Given Name	**Huynh Thanh**
	Prefix	
	Suffix	
	Role	
	Division	
	Organization	Vietnam National University-Ho Chi Minh City
	Address	Ho Chi Minh City, Vietnam
	Email	
Author	Family Name	**Huy**
	Particle	
	Given Name	**Dao Huu**
	Prefix	
	Suffix	

Role	
Division	
Organization	Ho Chi Minh City University of Technology and Education
Address	Ho Chi Minh City, Vietnam
Email	

Abstract	This article proposes a single-phase permanent magnet linear generator (PMLG) applied to a free piston engine (FPE) to produce electricity. It has an outer stator and an inner rotor (mover) that is driven by a motor with a linear frequency ranging from 10 to 50 Hz. The generator model has been simulated in 3-D using the Finite Element Method (FEM) through Ansoft Maxwell V16 (AM-V16) software to determine the magnetostatic properties. The MATLAB software is then utilized to obtain basic output parameters such as current, voltage, and power, using these parameters. The simulation and experimental results show that the voltage, current, and power differ insignificantly from 10 to 30 Hz. However, the difference is significant in the speed range from 40 to 50 Hz due to magnetic saturation. The peak power and efficiency are achieved at approximately 140 W and 81% with a load R_L = 10 Ω at a linear frequency of 50 Hz. The results from this study show that single-phase linear generators are completely applicable to power generation on FPE.

Keywords (separated by '-')	Permanent magnet linear generator—PMLG - Electromagnetics analysis - Finite Element Method—FEM

Preliminary Design of a Single-Phase Linear Generator for Free-Piston Engine Application

Nguyen Huynh Thi[1], Nguyen Van Trang[1(✉)], Huynh Thanh Cong[2], and Dao Huu Huy[1]

[1] Ho Chi Minh City University of Technology and Education, Ho Chi Minh City, Vietnam
trangnv@hcmute.edu.vn

[2] Vietnam National University-Ho Chi Minh City, Ho Chi Minh City, Vietnam

Abstract. This article proposes a single-phase permanent magnet linear generator (PMLG) applied to a free piston engine (FPE) to produce electricity. It has an outer stator and an inner rotor (mover) that is driven by a motor with a linear frequency ranging from 10 to 50 Hz. The generator model has been simulated in 3-D using the Finite Element Method (FEM) through Ansoft Maxwell V16 (AM-V16) software to determine the magnetostatic properties. The MATLAB software is then utilized to obtain basic output parameters such as current, voltage, and power, using these parameters. The simulation and experimental results show that the voltage, current, and power differ insignificantly from 10 to 30 Hz. However, the difference is significant in the speed range from 40 to 50 Hz due to magnetic saturation. The peak power and efficiency are achieved at approximately 140 W and 81% with a load $R_L = 10\ \Omega$ at a linear frequency of 50 Hz. The results from this study show that single-phase linear generators are completely applicable to power generation on FPE.

Keywords: Permanent magnet linear generator—PMLG · Electromagnetics analysis · Finite Element Method—FEM

1 Introduction

Nowadays, the Permanent Magnet Linear Generator (PMLG) is considered a potential candidate for energy conversion devices that have linear frequency. Different from the traditional generator, PMLG employs variable linear motion rather than rotary motion, resulting in a simpler structure and minimal energy loss during the conversion process by eliminating redundant transmission devices [1–3]. With the rapid advancement of high energy density magnetic materials, PMLG is garnering increasing attention for numerous applications due to its enhanced power and reliability [4–6] such as regenerating energy from ocean waves [7–9]. Furthermore, the PMLG serves as a device that converts mechanical energy into electrical energy for use in the Free Piston Linear Engine (FPLE). This technology offers the benefits of decreasing harmful gas emissions [10] and achieving high efficiency by minimizing friction when compared to traditional heat engines. Its variable compression ratio makes it adaptable to a wide range of fuels [11–15]. Presently, the FPLE represents a focal point in research endeavors aimed at enhancing vehicle performance and extending range [16–19].

M. Pagac et al. (Eds.): SCFF 2024, LNNS 1062, pp. 1–10, 2024.
https://doi.org/10.1007/978-3-031-65656-9_17

This article uses a single-phase PMLG with a simple structure for various applications such as creating energy from ocean waves and free piston engines. The generator is designed and examined across a linear frequency range of 10–50 Hz, with a maximum linear displacement of – 20 to 20 mm. The 3D model of generator is simulated using the Finite Element Method (FEM) with AM-V16 to analyze magnetostatics. The simulation results obtained from AM-V16 are then inputted into MATLAB software to determine output parameters such as current, voltage, and power. Finally, the experimental results are compared to evaluate the reliability of the simulation results.

2 Construction of a Single-Phase Linear Generator Model

The article introduces a flat single-phase generator comprising two generating surfaces, with its three-dimensional structure depicted in Fig. 1. The initial dimensions of both the rotor (mover) and stator assemblies are detailed in Table 1 and illustrated in Fig. 2.

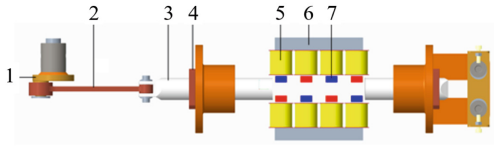

1 - Eccentric gear mechanism
2 - Connecting rod shaft
3 - Rotor
4 - Journal bearing
5 - Permanent magnet
6 - Coil ; 7 - Stator

Fig. 1. PMLG appled to FPE system

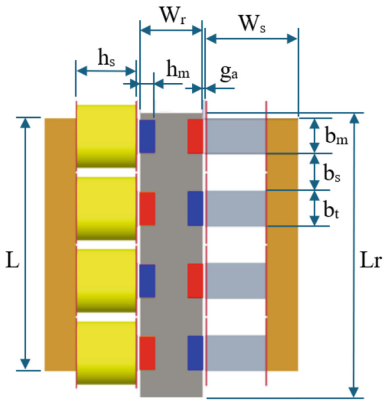

Fig. 2. Cross-sectional structure of PMLG

The PMLG comprises two main components: the rotor and the stator (mover). The rotor features two sides equipped with permanent magnets, with the polarization direction being opposite on the two opposing faces and alternating on the same face. Constructed from aluminum, the rotor is designed to minimize weight. Linear frequency motion is achieved through an eccentric gear mechanism, serving as a substitute for a

Table 1. Specification of PMLG

Variables	Symbol	Value
Stator width	W_s	40 mm
Length of the stator core	L	160 mm
Tooth width	bt	20 mm
Slot width	b_s	20 mm
Height of magnets	h_m	10 mm
Magnets width	b_m	20 mm
Tooth pitch	τ_t	40 mm
Tooth high	h_s	35 mm
Air gap	g_a	1 mm
Length of the rotor	L_r	180 mm
Rotor width	Wr	40 mm
Number of armatures	M_s	2
Number of turns per coil	N_{ph}	135 × 8 coil

free-piston engine. The permanent magnet section of the rotor is crafted from NdFeB rare earth magnets. Horizontal motion of the rotor is facilitated by a motor with a maximum power output of 1.1 kW. The outer stator consists of two multilayer ferrite cores aligned in parallel with the permanent magnets' surfaces. A 1mm clearance is maintained between the magnet and the stator. Each ferrite core is segmented into four teeth, encircled by wound coils. The copper wire's diameter is set at 1.5mm, with 135 turns of wire per tooth.

3 Simulation Study

3.1 Basic Parameters of the Generator

The functioning of a PMLG is grounded in electromagnetic induction and linear motion motor principles. When a magnet is attached to a rotor, it induces a consistent alteration in the magnetic field across the coil, thereby creating electromotive force and resulting in alternating current as the output. The electromechanical characteristics of the generator are significantly affected by the core sizes and winding parameters. To solve this problem, the AM-V16 is used to address all concerns related electrostatics, which are stated in Maxwell's differential equations.

The basic principles governing permanent magnet linear generators are derived from Maxwell's equations, especially those relating to magnetic fields.

From Ampere's law:

$$\nabla \times H = J \tag{1}$$

where J is the current density, H is the field intensity.

According to Gauss law:

$$\nabla \times \mathrm{B} = 0 \tag{2}$$

where B is the magnetic flux density.

Magnetic flux density B can be related to H as:

$$\mathrm{B} = \mu \times \mathrm{H} \tag{3}$$

where μ is the material permeability.

If the material is nonlinear, the permeability is a function of B:

$$\mu = \frac{B}{H} \tag{4}$$

The magnetic flux density B can be expressed in terms of the potential energy vector A as follows:

$$\mathrm{B} = \nabla \times \mathrm{A} \tag{5}$$

where A is the magnetic vector potential.

From Eqs. (4) and (5), it is obtained:

$$\nabla \times \left(\frac{1}{\mu(B)} \times A \right) = 0 \tag{6}$$

The FEM is a numerical technique used to solve Eq. (6), especially for static problems with nonlinear B-H relationships. Figure 3 illustrates the simulated model generated using AM-V16.

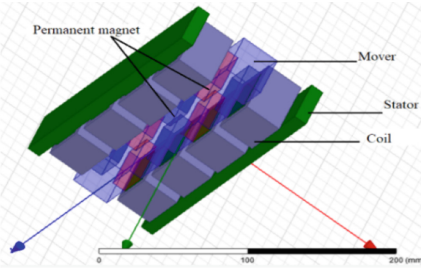

Fig. 3. Simulation model on AM-V16

The simulation results depicted in Fig. 4 indicate that the maximum flux passing through the coil is Br = 1.3T. The magnetic force lines form a closed loop around the coil, thereby generating an induced electromotive force.

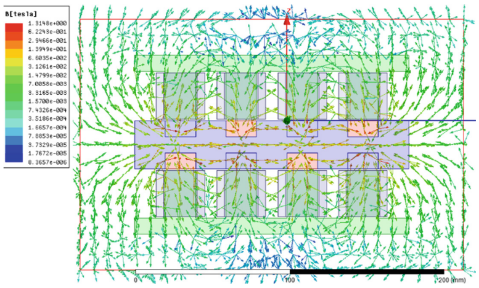

Fig. 4. Direction vector B

3.2 Output Parameters Calculation of Generator

The simulation parameters obtained from FEM, along with the geometric parameters determined in Table 1 will be imported into MATLAB software to model the output parameters of generator. The purpose of the simulation is to determine the current, voltage and power characteristics under a resistive load of RL = 10 Ω. The armature resistance is determined to be Ra = 0.25 Ω and the synchronous inductance of the coil is expressed as Ls = 0.105 H, with all parameters taken from experimental data. The performance of a single-phase generator operating at constant speed is then tested using the equivalent circuit depicted in Fig. 5.

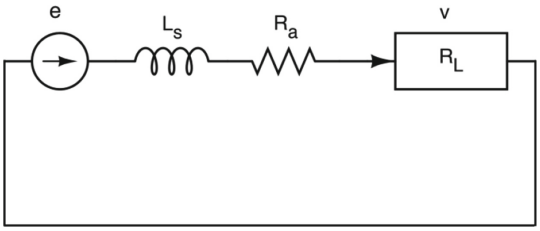

Fig. 5. Equivalent circuit of a single-phase generator winding

The Carter coefficient calculates the equivalent clearance [20]:

$$K_c = \frac{\tau_t(5ga + b_s)}{\tau_t(5ga + b_s) - b_s^2} \tag{7}$$

where g_a is the air gap between the rotor and stator, b_s is the slot width; τ_t is the tooth pitch, it may be expressed as the sum of the slot width b_s and tooth width b_t.

The equivalent air gap is calculated:

$$g_{eq} = K_C \times g_a \tag{8}$$

The air gap flux density, taking into account the increase in reluctance, can be expressed as follows:

$$\emptyset = \frac{B_r h_m H_c \mu_0}{h_m H_c \mu_0 - g_{eq} B_r} \tag{9}$$

where Br represents the allowable magnetic flux density in the translator core t, Hc = 90,5000 A/m represents the forced magnetic field intensity, and Hm represents the height of the magnet. The permeability of free space, denoted as μ_0: $\mu_0 = 4\pi \times 10 - 7$ T.m/A.

In Fig. 5, the values of phase induced voltages is:

$$e = R_a \times i + L_s \frac{di}{dt} + V \tag{10}$$

where R_a is the armature resistance, L_s is the synchronous inductance, V is the voltage (V), and i is the current (A).

$$V = i \times R_L \tag{11}$$

where R_L is the resistive load.

The induced voltages in the windings for single-phase is:

$$e_{ph} = K_E \times \cos(\frac{\pi}{\tau} z) \times v(t) \tag{12}$$

where z is the uniformly variable displacement of the mover:

$$z = A \times \sin(2\pi ft - \frac{\pi}{2}) \tag{13}$$

where A represents the displacement of the mover, and f denotes the frequency of the displacement movement.

Speed of the mover v(t) is:

$$v(t) = z' = 2\pi \times A \times f \times \cos(2\pi ft - \frac{\pi}{2}) \tag{14}$$

$$K_E = M_s \times W_s \times N_{ph} \times \Phi \times v_{av} \tag{15}$$

where M_s is the number of armatures, W_s is the stator width, N_{ph} is the number of turns per coil, v_{av} is the average speed of the mover.

Differential equation for phase current

$$\frac{di}{dt} = \frac{e - v - i \times R_a}{L_s} \tag{16}$$

$$\text{The power : } P_{out} = e_{ph} \times i \tag{17}$$

The displacement with maximum speed from 1 to 6 m/s corresponding to from 10 to 50 Hz.

4 Simulation and Experimental Results

Using the design data and simulation outcomes, an experimental prototype of the PMLG is developed. The linear motion of the mover is driven by a 1.1 kW motor through an eccentric gear mechanism. To adjust the linear frequency and monitor the voltage and current parameters of the motor, the VEICHI AC10 inverter is employed. The experimental arrangement is illustrated in Fig. 6. Experimental data is collected using the dedicated pulse meter X431TOP, equipped with 4 channels, a maximum frequency of 20 MHz, and capable of measuring voltages up to ± 150 V.

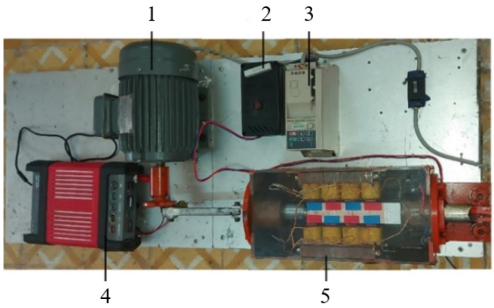

1 - Motor
2 - Load resistor
3 - Inverter
4 - Oscilloscope
5 - Linear generator

Fig. 6. Experimental model of PMLG

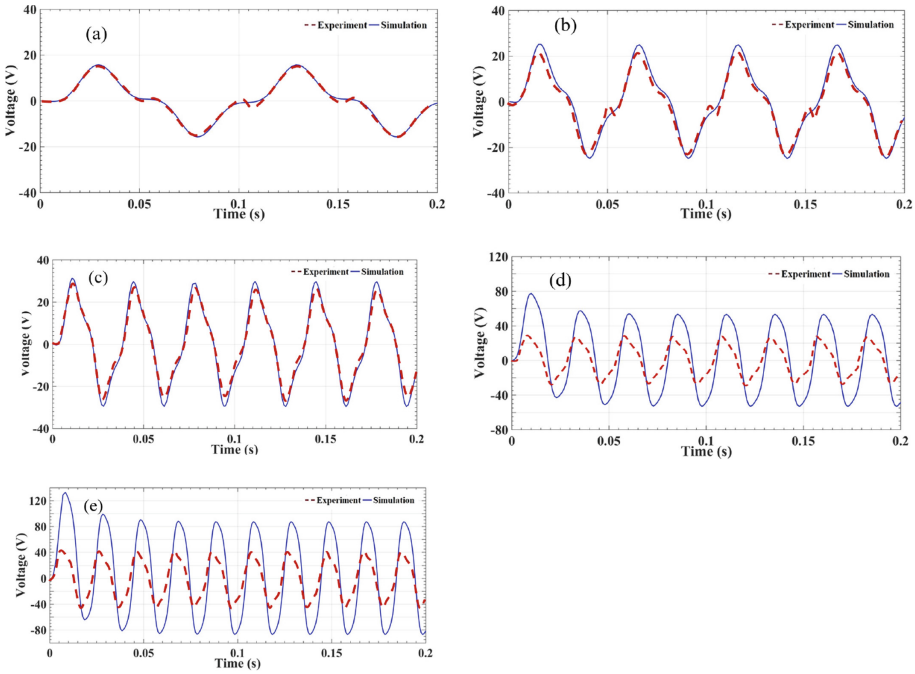

Fig. 7. Voltage waveform of the simulation and experimental results at linear frequency of 10 Hz (a), 20 Hz (b), 30 Hz (c), 40 Hz (d), and 50 Hz (e)

The simulation and experiment have been performed to compare and analyze voltage, current, and power parameters based on load $R_L = 10\ \Omega$ and different frequencies, the frequency is set as 10 Hz, 20 Hz, 30 Hz, 40 Hz, and 50 Hz respectively.

Displacement of PMLG is restricted from $-$ 20 to 20 mm. The waveforms of the simulation and experiment are almost the same, there are still small deviations because the speed mover is difficult to control precisely due to the inertia force. The limit of the operation is 50 Hz because of the highest speed of the motor and the mechanical

strength. The simulation results are compared with those experimental results under the same conditions and are shown in Fig. 7.

When the piston frequency increases from 10 to 30 Hz corresponding to the speed of motor movement increasing from 1 to 3 m/s, the voltage increases rapidly from 15 to 30 V according to experimental data and from 17 to 38 V according to the data simulation. In this period, the experimental and simulation do not have much difference, the same for current, and power. The linear frequency from 40 to 50 Hz corresponds to the maximum speed of the motor from 3 to 6 m/s, simulated voltage increased from 60 to 90 V, current increased from 3.5 to 8 A, and peak power at 50 Hz = 720 W. However, the experimental results show that the parameters of the generator insignificantly increased, the voltage increased from 35 to 40 V, and the current increased from 2.8 to 3.5 A with peak power of 140 W at 50 Hz. Current and power are shown in Fig. 8, the magnetic saturation of the generator has reached the limit.

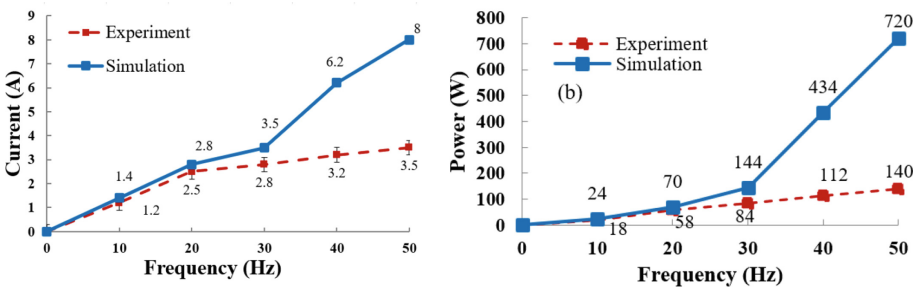

Fig. 8. Current (a) and power (b) at different frequencies

In this model, the generator efficiency is calculated:

$$h = \frac{W_g}{W_m} \times 100\% \tag{18}$$

where W_g is the efficiency of the generator, W_m is the power of the motor used to drive the mover and W_m is collected directly on the inverter $W_m = 171$ W at a linear frequency 50 Hz. Thus, efficiency is $h \approx 81\%$ at 50 Hz power loss due to mechanical friction and magnetic through the air gap.

The displacement speed of the mover can change the determination of voltage, current, and power. In addition, reducing the armature resistance R_a and the synchronous inductance of the coil L_s can increase the power of the PMLG, but this depends on the quality of the winding material. On the one hand, because the generator uses a permanent magnet, magnetic saturation occurs, so to increase the power of the generator, it is recommended to use an electromagnet instead of a permanent magnet or use a linear generator 3-phase.

5 Conclusion

This paper introduces a single-phase PMLG structure tailored for. This paper introduces a single-phase PMLG structure specifically designed for Free Piston Linear Engines (FPLEs). It presents 3D schematics, experimental models, and dimensional parameters. Using the Finite Element Method (FEM), simulation parameters including flux distribution density and inductance were obtained using both Ansoft Maxwell V16 and MATLAB software. These simulations are instrumental in determining the power and current characteristics of the PMLG. The simulation and experimental results align closely over the frequency range of 10–30 Hz, showcasing linear increases in voltage, current, and power parameters. However, discrepancies emerge at higher frequencies, specifically from 40 to 50 Hz, attributable to magnetic saturation effects. Peak power and efficiency are attained at approximately 140 W and 81%, respectively, under a load of $R_L = 10\ \Omega$ at a linear frequency of 50 Hz. The experiments therefore demonstrate the suitability of this structure for low-frequency linear oscillation applications, such as ocean wave energy regeneration, free piston engine energy conversion and energy recovery from car vibrations.

References

1. Zou, J., Zhao, M., Wang, Q., Zou, J., Wu, G.: Development and analysis of tubular transverse flux machine with permanent magnet excitation. IEEE Trans. Ind. Electron. **59**(5), 2198–2207 (2012)
2. Jing, H., Maki, N., Ida, T., Izumi, M.: Electromechanical design of an MW class wave energy converter with an HTS tubular linear generator. IEEE Trans. Appl. Supercond. **28**(4), Art. no. 4902504 (2018)
3. Huang, L., Hu, B., Hu, M., Liu, C., Zhu, H.: Research on primary excitation fully superconducting linear generators for wave energy conversion. IEEE Trans. Appl. Supercond. **29**(5), Art. no. 5203405 (2019)
4. Gandhi, A., Parsa, L.: Thrust optimization of a five-phase fault-tolerant flux-switching linear synchronous motor. In: Proceedings of IEEE Industrial Electronics Society Conference, pp. 2067–2073 (2012)
5. Chen, H., Zhan, Y., Wang, H., Nie, R.: A tubular permanent magnet linear generator with novel structure. IEEE Trans. Plasma Sci. **47**(6), 2995–3001 (2019)
6. Chen, H., Zhan, Y., Wang, H., Nie, R.: A novel single-phase tubular permanent magnet linear generator. IEEE Trans. Appl. Superconduct. **30**(4), Art. no. 5202705 (2020)
7. Hodgins, N., Keysan, O., McDonald, A.S., Mueller, M.A.: Design and testing of a linear generator for wave-energy applications. IEEE Trans. Ind. Electron. **59**, 2094–2103 (2012)
8. Kimoulakis, N.M., Kladas, A.G., Tegopoulos, J.A.: Power generation optimization from sea waves by using a permanent magnet linear generator drive. IEEE Trans. Magn. **44**(6), 1530–1533 (2008)
9. Hanipah, M.R., Mikalsen, R., Roskilly, A.P.: Recent commercial free-piston engine developments for automotive applications. Appl. Therm. Eng. **75**, 493–503 (2015)
10. Feng, H., Guo, C., Jia, B., Zuo, Z., Guo, Y., Roskilly, T.: Research on the intermediate process of a free-piston linear generator from cold start-up to stable operation: numerical model and experimental results. Energy Convers. Manage. **122**, 153–164 (2015)
11. Hansson, J., Leksell, M: Performance of a series hybrid electric vehicle with a free-piston energy converter. IEEE Xplore (2007)

12. Mikalsen, R., Roskilly, A.P.: A review of free-piston engine history and applications. Appl. Therm. Eng. **27**, 2339–2352 (2007)
13. Jia, B., Mikalsen, R., Smallbone, A., Paul Roskilly, A.: A study and comparison of frictional losses in free-piston engine and crankshaft engines. Appl. Therm. Eng. (2018)
14. Mikalsen, R., Roskilly, A.P.: The control of a free-piston engine generator, part 1: fundamental analyses. Appl. Energy **87**, 1273–1280 (2010)
15. Yuan, C., Jing, Y., Liu, C., He, Y.: Effect of variable stroke on fuel combustion and heat release of a free piston linear hydrogen engine. Int. J. Hydrogen Energy **44**, 20416–20425 (2019)
16. Vysoký, O.: Linear combustion engine as main energy unit for hybrid vehicles. In: Proceedings of Transtec Prague. Prague: Czech Technical University, pp. 236–244 (2007)
17. Lim, O., Hung, N.B., Oh, S., Kim, G., Song, H., Iida, N.: A study of operating parameters on the linear spark ignition engine. Appl. Energy **160**, 746–760 (2015)
18. Li, L., Luan, Y., Wang, Z., Deng, J., Wu, Z.: Simulations of key design parameters and performance optimization for a free-piston engine. In: SAE, p. 1105 (2010)
19. Sun, P., et al.: Hybrid system modeling and full cycle operation analysis of a two-stroke free-piston linear generator. Energies **10**, 213 (2017)
20. F. W. Carter.: Air-gap induction. Electr World Eng. **38**(22), 884–888 (1901)

AQ1

Author Queries

Chapter 17

Query Refs.	Details Required	Author's response
AQ1	Kindly note that references [10] and [11] are same, we have deleted the duplicate reference and renumbered accordingly. Please check and confirm.	